



# 1 **Hyper-Resolution Land Surface Modeling for Farm-Scale Soil** 2 **Moisture in India: Enhancing Simulations with Soil Vertical** 3 **Heterogeneity**

4 Vishnu U Krishnan<sup>1</sup>, Noemi Vergopalan<sup>4</sup>, Bhupendra Bahadur Singh<sup>5</sup>, Jayaluxmi Indu<sup>1,3</sup>, Lanka Karthikeyan<sup>1,2\*</sup>  
5 <sup>1</sup>Center for Climate Studies, Indian Institute of Technology Bombay, Mumbai, 400076, India  
6 <sup>2</sup>Centre of Studies in Resources Engineering, Indian Institute of Technology Bombay, Mumbai, 400076, India  
7 <sup>3</sup>Department of Civil Engineering, Indian Institute of Technology Bombay, Mumbai, 400076, India  
8 <sup>4</sup>Rice University, Department of Earth, Environmental and Planetary Sciences, Houston, TX, USA  
9 <sup>5</sup>Centre for Climate Change Research, Indian Institute of Tropical Meteorology, Ministry of Earth Sciences,  
10 Government of India, Pune, 411008, India  
11 \*Correspondance to: L. Karthikeyan ([karthikl@iitb.ac.in](mailto:karthikl@iitb.ac.in))

12 **Abstract:** Estimation of field-scale surface and rootzone soil moisture (SM) is crucial for agriculture water  
13 management. When ground observations are not available, Land Surface Models (LSMs) aid in reconstructing  
14 historical dynamics and providing predictions. However, they often run at coarse resolution (in the order of tens  
15 of kilometers), overlook subgrid processes (e.g., lateral flow), and thus underestimating the SM spatial  
16 heterogeneity. Considering this limitation, we applied the Noah-MP LSM with the HydroBlocks hyper-resolution  
17 modeling framework to estimate surface and rootzone SM at field scale (effective 30 meters resolution) for the  
18 first time in India. Recognizing the importance of rootzone processes for agriculture, the present study attempts  
19 to improve high-resolution rootzone SM simulations by incorporating vertical heterogeneity in soil properties into  
20 HydroBlocks using the SoilGrids global soil database. The analysis is carried out in Upper Bhima Basin (a  
21 subbasin of Krishna Basin) for 2020 with ERA5-Land meteorological forcing.  
22 HydroBlocks simulations, configured with vertically homogeneous (VHom) and vertically heterogeneous (VHet)  
23 soil properties, were compared against GLEAM, ERA5-Land, SMAP-L3, and SMAP-L4, revealing temporal  
24 consistency (correlation between 0.76 and 0.94) and improved sub-grid (up to  $0.2 \text{ m}^3\text{m}^{-3}$ ) and spatial variability  
25 ( $\sigma_0$ ), in particular VHet ( $\sigma_0 = 0.093 \text{ m}^3\text{m}^{-3}$ ) higher than VHom ( $\sigma_0 = 0.09 \text{ m}^3\text{m}^{-3}$ ). Both HydroBlocks  
26 configurations show reasonable performance against in situ SM observations, with VHet showing systematic  
27 improvement compared to VHom by reducing the bias in all sub surface layers and a higher correlation (0.60)  
28 than VHom (0.59) at deeper layer (0-60 cm). Finally, we performed a Sobol sensitivity analysis to investigate the  
29 seasonal sensitivity of soil on HydroBlocks (VHet) SM simulations for the first five soil layers (up to 1 meter  
30 depth). Results revealed that soil parameters interact more prominently in the surface layer and during monsoons.  
31 Soil porosity (MAXSMC), Brooks-Corey parameter (BB), and SM at wilting point (WLTSMC) are significant  
32 parameters across seasons. Their order of significance changes from surface to deeper layers; however, they  
33 remain consistent beyond 30 cm depth. This study finds that the hyper-resolution LSM with vertical soil  
34 heterogeneity can enhance small-scale SM simulations by accounting for varying parameter importance,  
35 interactions, and seasonal effects within the soil column.

## 36 **1. Introduction**

37 Soil moisture is an important state variable in the energy and water cycles. It effectively controls sensible and  
38 latent heat fluxes at the land-atmosphere interface (Benson and Dirmeyer, 2021), playing a decisive role in land-  
39 atmospheric interactions (Schwingshackl et al., 2018; Sehgal et al., 2021; Goswami et al., 2023). Soil moisture



40 available at the plant root zone (up to 1 m deep from the surface) represents the water availability to plants. Hence,  
41 rootzone soil moisture is significant in agriculture (Rigden et al., 2020; Tjrdeman and Menzel, 2021). There is a  
42 notable spatial scale dependency on soil moisture variability, which is attributed to physical controls, including  
43 climatic factors like precipitation and land surface variability due to soil types, vegetation characteristics, and  
44 topography (Famiglietti et al., 2008; Gaur and Mohanty, 2016; Rosenbaum et al., 2012; Vergopolan et al., 2022).  
45 The dominance of these soil moisture controls varies significantly with changing spatial scales (Joshi and  
46 Mohanty, 2010; Vergopolan et al., 2022). With an increase in spatial resolution (from 25 km to ~1.6 km), drivers  
47 of soil moisture variability shift from vegetation, soil, and topography (Gaur and Mohanty, 2013, 2016) to mostly  
48 soil itself. Accordingly, the significance of scale and spatial variability may vary depending on the emphasis of  
49 different studies. The landscape heterogeneity is further enhanced by farming practices (irrigation, fertilizer  
50 application, tile drainage) (Vergopolan et al., 2021; Yang et al., 2024), particularly at the surface layer. This  
51 heterogeneity is not captured within a coarser grid resolution and is even more challenging to assess in a  
52 fragmented agrarian system (Vergopolan et al., 2021).

53 Land surface Models (LSMs) have advantages over satellite and point scale observations by providing temporally  
54 consistent hydrologic estimates over a large extent. Although LSMs are capable of accurate simulation of various  
55 land surface processes, traditional models are limited to macro scales (in the order of tens of kilometers), which  
56 are primarily intended to run synergistically with climate models (Ek et al., 2003; Lawrence et al., 2011; Niu et  
57 al., 2011). The coarse resolution can overlook many aspects of agricultural applications, including irrigation water  
58 management and crop yield prediction (Ray et al., 2022). However, traditional LSMs still overlook many subgrid  
59 processes, including subsurface lateral connectivity, which becomes significant when the model resolution  
60 becomes finer (Ji et al., 2017; Kim and Mohanty, 2016; Krakauer et al., 2014; Singh et al., 2015). To understand  
61 the soil moisture heterogeneity at the farm scale (in the order of a few meters), LSMs must accurately represent  
62 the complexity of various land surface processes at that scale. However, increasing complexity significantly  
63 increases computational expenses.

64 HydroBlocks (Chaney et al., 2016, 2021) is a semi-distributed hyper-resolution (< 1 km) LSM with Noah-MP at  
65 its core intended to simulate soil moisture at 30 m spatial resolution. One of the critical advantages of HydroBlocks  
66 is its incorporation of subsurface lateral connectivity between its computing units. Studies have been conducted  
67 to leverage the benefits of this semi-distributed modeling approach to simulate soil moisture at hyper-resolution  
68 without making the simulations computationally expensive (Torres-Rojas et al., 2022; Vergopolan et al., 2020,  
69 2021). In India, fragmented agriculture prevails with 86% small or marginal holdings with farm sizes less than 2  
70 hectares (Agriculture Census, 2015-16). Hence, considering the backdrop of small farm sizes prevalent in the  
71 country, representing sub-grid heterogeneity of soil, topography, and meteorological variables at the field scale is  
72 fundamental. High resolution soil moisture aids agricultural applications, including drought (Park et al., 2017;  
73 Vergopolan et al., 2021), crop yields (Vergopolan et al., 2021), precise irrigation and water management (Jalilvand  
74 et al., 2021, 2023; Zhou et al., 2024).

75 However, one of the critical challenges to extending the applicability of a hyper-resolution LSM is the availability  
76 of high-resolution input data as well as point scale observations for validation. The availability of digital soil maps  
77 at a finer spatial resolution and applying Pedo Transfer Functions (PTFs) for estimating soil-hydraulic properties  
78 can provide better results for surface soil moisture simulations compared to the traditional look-up table approach  
79 in the LSMs (Xu et al., 2023). Soil properties are dominant physical controls in soil moisture spatial heterogeneity



80 (Crow et al., 2012; Vergopolan et al., 2022). The importance of incorporating soil vertical heterogeneity in LSMs  
81 is emphasized in previous studies either through a simplified LSM considering a single soil column (Yang et al.,  
82 2005) or approximating effective hydraulic parameters (Zhu and Mohanty, 2003). While those approaches were  
83 valuable in advancing our understanding, their application in simulating soil moisture at a heterogeneous land  
84 surface at field scales covering large spatial extent remains limited. Incorporating soil vertical heterogeneity in  
85 the HydroBlocks LSM has improved field scale surface soil moisture simulation (Xu et al., 2023). However, the  
86 effects of incorporating soil vertical properties in the model to simulate rootzone soil moisture at the field scale  
87 are still unknown. With the greater significance of rootzone soil moisture in agriculture, a study on understanding  
88 the role of soil vertical properties on rootzone soil moisture simulations applied agriculture-dominant countries  
89 like India is needed

90 The soil hydraulic properties are parameterized in LSMs, and uncertainties in these soil parameters affect soil  
91 moisture simulations (Arsenault et al., 2018; Cai et al., 2014). Applying PTFs on digital soil maps and  
92 incorporating soil vertical properties offers a better representation of the spatial heterogeneity of soil parameters.  
93 Besides, HydroBlocks LSM, which accounts for subsurface lateral flow, can provide more accurate field scale  
94 soil moisture simulations (Vergopolan et al., 2022, 2020). However, the vertical and seasonal influence on these  
95 properties in soil moisture simulation at the field scale remains unknown. Hence, a detailed sensitivity analysis  
96 of soil parameters on soil moisture simulations at a field scale is required.

97 The current study deploys digital soil maps combined with PTFs to estimate soil properties for each vertical soil  
98 layer in HydroBlocks and soil moisture at the farm scale (30 m spatial resolution). Although the primary goal of  
99 this study is to understand the effect of soil vertical properties in rootzone soil moisture, a study emphasizing the  
100 importance of having hyper-resolution LSM in India is still missing. For the first time, a hyper-resolution LSM  
101 simulations were set up over an Indian catchment, the Upper Bhima basin, a sub-basin of Krishna, in Maharashtra..  
102 Although focused on a single catchment, this research holds global relevance, particularly considering that 84%  
103 of the world's farmers are smallholders.

104 The current study evaluates the performance of surface and rootzone soil moisture simulations obtained from two  
105 configurations of HydroBlocks – the first configuration with vertically heterogeneous soil properties and the  
106 second with vertically homogeneous soil properties. The soil moisture simulations from the model are evaluated  
107 using available in situ soil moisture station data in the basin at multiple soil depths. Because India does not have  
108 a well-monitored soil moisture network to evaluate the simulations, we also assessed the performance using  
109 satellite and reanalysis of soil moisture products. We also did an intercomparison between two HydroBlocks  
110 configurations at multiple layers (up to 1 m deep) to simulate soil moisture at each layer. Besides, a comprehensive  
111 understanding of the significance of soil parameters in hyper-resolution modeling of soil moisture for each soil  
112 layer and their seasonal variability remains unknown. Hence, for the first time, we performed a global sensitivity  
113 analysis test using the HydroBlocks, which considers soil vertical heterogeneity, on five soil layers (up to 1 meter  
114 depth) to assess the influence of soil textural parameters on the model simulated soil. In this process, we also  
115 evaluated the seasonal variability of parameter sensitivity. Through this research, we aim to address the following  
116 research questions:

- 117     ▪ What are the benefits of a hyper-resolution LSM in generating soil moisture at the surface and rootzone  
118         over an agriculture-dominant landscapes in India?

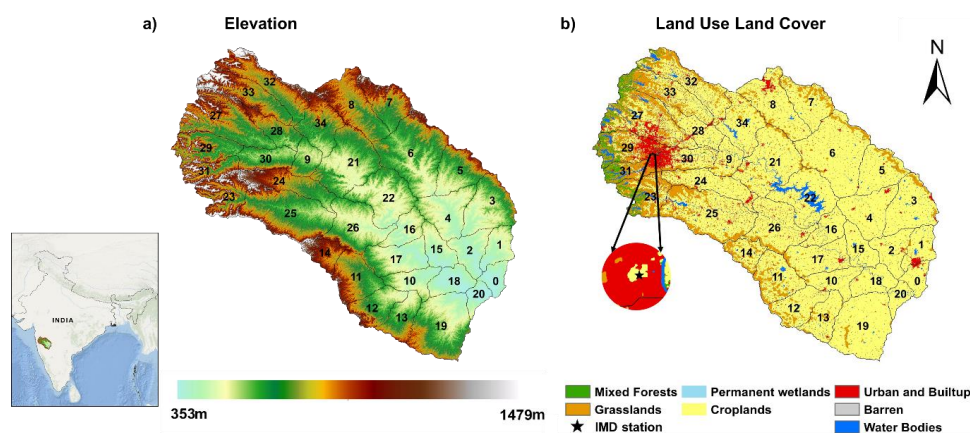


- 119       ▪ What changes does the integration of vertical soil heterogeneity into the model bring in the simulation  
120           of surface and rootzone soil moisture?  
121       ▪ What are the sensitive soil parameters toward soil moisture in each soil layer?  
122       ▪ Is there a seasonal influence on the soil parameter sensitivity?

## 123 2. Data and Methods

### 124 2.1 Study Area

125 The present study is carried out in the Upper Bhima basin, as shown in Fig.1, a subbasin of the Krishna Basin in  
126 India. The Upper Bhima basin has a spatial extent spread around 45,790 km<sup>2</sup> between 73.3° and 76.10° longitudes  
127 and 16.85° and 19.40° latitudes. The terrain is characterized by high elevation (353 m -1479 m) with steep slopes  
128 towards the west and flat land towards the east. The subbasin is identified with seven land cover classes according  
129 to IGBP standards of land cover classification, as shown in Fig.1. The majority of the basin area is occupied by  
130 croplands with more than 77%, followed by grasslands (12%), urban and built-up areas (6%), water bodies (2.5%),  
131 mixed forests (1.8%), with the remainder 0.7% for barren lands and permanent wetlands.  
132



133  
134 **Figure 1:** The Upper Bhima Basin (a) elevation in meters and (b) land use land cover (LULC) according to IGBP  
135 classification. The basin is divided into 35 subwatersheds modeled independently. The inset shows the location  
136 of the IMD station for in situ soil moisture observations.

137 The entire study area is subdivided into 35 watersheds (Lehner and Grill, 2013), with area varying between 490  
138 km<sup>2</sup> and 2883 km<sup>2</sup> to make the simulations computationally feasible. The climate of the Upper Bhima River  
139 Basin is marked by a high degree of variability due to the interplay between the monsoon and the Western Ghat  
140 mountain range (Gunnell, 1997) The average annual rainfall for the basin is 653 mm, which is distributed non-  
141 uniformly across space and time (Garg et al., 2012). The Western Ghats zone receives heavy rainfall, with a  
142 maximum of 5000 mm per year. However, the rainfall decreases significantly towards the eastern slopes and  
143 plateau areas, falling below 500 mm per year (Pavelic et al., 2012).



144 **2.2 Data**

145 **2.2.1 ERA5-Land**

146 ERA5-Land is the fifth-generation global reanalysis product, providing hourly data for the land component of  
147 ERA5 at a spatial resolution of 9 km from 1950 onwards (Muñoz-Sabater et al., 2021). The model assimilates  
148 data from satellite sensors like Soil Moisture Ocean Salinity (SMOS), Advanced Microwave Scanning  
149 Radiometer-2 (AMSR-2), Tropical Rainfall Measuring Mission Microwave Imager (TRMM-MI), Active  
150 microwave instrument scatterometer onboard ERS1/2 and meteorological operational satellite for soil moisture  
151 product. Soil moisture data available at three soil layer depths (0-7 cm, 7-28 cm, and 28-100 cm) at 3-hour  
152 intervals were used in the current study for comparison with the model simulated soil moisture data.

153 **2.2.2 GLEAM**

154 GLEAM is a set of algorithms that estimate the main components of evapotranspiration based on satellite  
155 observations (Martens et al., 2017). In the current study, we have used GLEAM v3.6a – a global dataset spanning  
156 42 years with a spatial resolution of 0.25° and a temporal resolution of 1 day. This dataset is based on the reanalysis  
157 radiation and air temperature, a combination of gauge-based reanalysis and satellite-derived precipitation and  
158 satellite derived vegetation optical depth. Soil moisture data from this product is available for surface (0-10 cm)  
159 and (0-100cm)

160 **2.2.3 SMAP enhanced L3**

161 The Soil Moisture Active Passive (SMAP) enhanced Level 3 product is a daily composite based on SMAP  
162 enhanced Level 2 product (O'Neill et al., 2021), providing global soil moisture data at a spatial resolution of 9 km  
163 available from 2015 onwards. In the current study, we have used daily SPL3SMP\_E, Version 5 soil moisture data  
164 (0- 5 cm) for the study area.

165 **2.2.4 SMAP L4**

166 The level-4 SMAP is a global product that merges SMAP observations into the NASA Catchment Land Surface  
167 Model (Reichle et al., 2014) using an Ensemble Kalman filter. Hence, it provides data at a deeper layer, facilitating  
168 rootzone soil moisture estimates. For the current study, we have used rootzone (0-100 cm) soil moisture estimates  
169 of SMAP L4 product at a spatial resolution of 9 km and temporal resolution of 3 hours.

170 **2.2.5 In-situ soil moisture data**

171 The India Meteorological Department (IMD) Agromet Division provides weekly soil moisture measurements for  
172 41 stations across India at various depths: 5 cm, 7.5 cm, 15 cm, 30 cm, 45 cm, and 60 cm based on gravimetric  
173 measurements. The Upper Bhima basin has only one station at 18.5385° N, 73.8429° E (Fig.1). However, during  
174 2020, due to the COVID-19 pandemic, soil moisture was recorded for only 34 weeks. Despite limited data, this  
175 comprises the best ground truth estimation of soil moisture in the domain.



176 **2.2.6 Data used in the HydroBlocks**

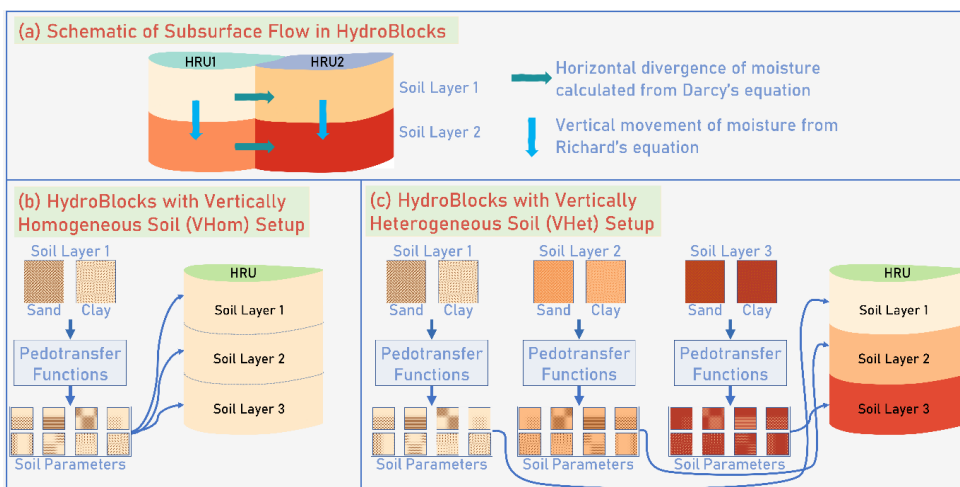
177 We use ERA5-Land (Muñoz-Sabater et al., 2021) as meteorological forcings, which include precipitation, air  
178 temperature, longwave and shortwave radiations, surface air pressure, wind speed, and specific humidity derived  
179 from 2 m dew point temperature at 0.1° spatial resolution and 3-h time intervals over a time period 2015-2020.  
180 Besides, the model also requires static data about soil characteristics, topography, and land cover regridded to 30  
181 m spatial resolution. We used the SoilGrids dataset (Hengl et al., 2017) at 250 m resolution and PTFs (Saxton and  
182 Rawls, 2006) to estimate other soil hydraulic properties. These include porosity, pore size distribution parameters,  
183 soil moisture at the wilting point, field capacity, saturated hydraulic conductivity, soil water diffusivity at  
184 saturation, and saturated soil matric potential. The land use land cover data is obtained from ESRI (Karra et al.,  
185 2021), available at 10 m resolution. Further, the land cover classes are reclassified based on IGBP classification  
186 as per the model requirement using the nearest neighbor for each 30m grid cell. The elevation data for topography  
187 is obtained from the ASTER Global Digital Elevation Model, available at a resolution of 30 m.

188 **2.3 HydroBlocks Model**

189 HydroBlocks (Chaney et al., 2016, 2021) is a semi-distributed hyper-resolution LSM that clusters areas of  
190 hydrologic similarity into Hydrologic Response Units (HRU). The HRUs form the domain's computing units and  
191 enable simulating land surface processes at an effective 30m spatial resolution. At its core, HydroBlocks applies  
192 Noah-MP to solve land surface processes within each HRU. The present study uses the HydroBlocks model  
193 version using Darcy's equation to maintain the lateral connectivity between HRUs at the subsurface (Chaney et  
194 al., 2021). HydroBlocks was validated over the United States and have been demonstrated to provide accurate and  
195 computationally feasible simulations of soil moisture at a farm scale (Vergopolan et al., 2021, 2020).

196 **2.4 HydroBlocks Model with Vertically Heterogenous Soil Parameterization for Soil Moisture Profile**  
197 **Simulations**

198 For computational efficiency, the basin was discretized into 35 sub-watersheds. For each sub-watersheds, we  
199 simulated soil moisture at 30 m resolution at the surface (0 – 5 cm) and the rootzone (0 – 100 cm) for the year  
200 2020 at a temporal resolution of 3 hours. We spin up the model from 2015 to 2019. In an attempt to improve the  
201 soil moisture profile simulations, the HydroBlocks model is modified to incorporate vertical heterogeneity in soil  
202 properties. The schematic of vertical heterogeneity implemented in HydroBlocks is shown in Fig.2. The vertical  
203 heterogeneity of soil properties corresponds to soil depth information as in SoilGrids, which are 0-5 cm, 5-15 cm,  
204 15-30 cm, 30-60 cm, 60-100 cm, and 100-200 cm. From this point forward, vertical heterogeneity (of soil  
205 properties) incorporated in HydroBlocks is referred to as HydroBlocks Vertically Heterogeneous (VHet) version.  
206 In the case of the existing model of HydroBlocks, the soil profile is assumed to be vertically homogeneous  
207 (VHom), wherein the surface layer soil properties are utilized for the entire soil column. Both model  
208 configurations are run at Noah-MP parameterization schemes, as shown in Table 1.



209  
 210 **Figure 2:** Schematics depicting HydroBlocks LSM setups. a) HydroBlocks updates soil moisture between  
 211 different soil layers after incorporating vertical flow between layers and lateral flow between the HRUs at the  
 212 subsurface layer for every timestep. The lateral subsurface flow is defined by Darcy's equation. b) HydroBlocks  
 213 model setup with vertically homogeneous (VHom) soil and after incorporating vertical heterogeneous (VHet) soil.  
 214 Soil properties for each layer are defined by sand clay and organic matter content using PedoTransfer Functions  
 215 (PTFs). Each small square represents soil parameters for each soil layer. Hence, the VHet setup has eight soil  
 216 parameters stacked for three soil layers (represented by three colours). In the VHom setup, the eight soil  
 217 parameters corresponding to the surface layer are used in the entire soil column.

218 **Table 1.** Description of the selected Noah-MP schemes

Parametrization	Schemes selected
Dynamic vegetation	Off
Canopy stomatal resistance	Ball-Berry
Soil moisture factor for stomatal resistance	Noah type
Runoff and groundwater	TOPMODEL-based scheme with the equilibrium water table
Surface layer drag coefficient	Monin-Obukhov-based
Supercooled liquid water in frozen soil	Koren99 scheme
Frozen soil permeability	Koren99 scheme
Radiation transfer	Modified two-stream
Ground snow surface albedo	CLASS
Snow/soil temperature time scheme (layer 1)	Semi implicit scheme

## 219 2.5 Performance Evaluation

220 To compare model simulations with IMD in situ soil moisture observations, we selected common depths (5 cm,  
 221 15 cm, 30 cm, and 60 cm). Soil moisture simulations from the model are hence calculated corresponding to layers  
 222 0- 5cm, 0-15 cm, 0-30 cm, and 0-60 cm after assigning weights based on the model layers 0-5 cm, 5-15 cm, 15-  
 223 30 cm, and 30-60 cm. VHet and VHom simulations are evaluated against in situ observations using bias, unbiased  
 224 Root Mean Square Error (ubRMSE), Pearson's correlation (R), and Spearman's rank ( $R_{sp}$ ) correlations.  
 225 Due to the limited availability of in situ soil moisture observations over the study area, HydroBlocks simulated  
 226 soil moisture is also compared with existing satellite and reanalysis products. These products include SMAP L3



227 Enhanced (9 km resolution), SMAP L4 (9 km resolution), ERA5-Land (0.1° resolution) and GLEAM (0.25°  
228 resolution). The evaluation of surface and rootzone soil moisture simulations is carried out in two ways. First,  
229 consistency with respect to satellite and reanalysis datasets is carried out in terms of temporal and spatial  
230 variations. Time variations are assessed in four randomly selected watersheds (Fig.S1). Spatial variations are  
231 evaluated in terms of daily soil moisture and spatial standard deviations (to analyze the subgrid heterogeneity).  
232 Spatial standard deviation is computed using the HydroBlocks simulations from grid cells falling within the  
233 coarser resolution grids of each reanalysis and satellite data. Second, a quantitative comparison is carried out by  
234 upscaling HydroBlocks soil moisture simulations to a reference macroscale product. We use bias, Pearson  
235 Correlation, and ubRMSE for this purpose. For the surface layer, spatio-temporal comparisons are carried out  
236 with SMAP L3, ERA5-Land, and GLEAM surface soil moisture. For the rootzone, SMAP L4, ERA5-Land, and  
237 GLEAM rootzone soil moisture are used for this purpose. In both cases, one SMAP grid cell is randomly identified  
238 within the four selected watersheds (Fig.S1), and soil moisture corresponding to the grid cell is considered from  
239 all datasets. A quantitative comparison is carried out using SMAP L3 and SMAP L4 as references for surface and  
240 rootzone soil moisture simulations.

## 241 2.6 Sensitivity Analysis

242 Soil moisture has high spatial-temporal variability. Understanding this variability in the context of the influence  
243 of soil textural properties requires a careful study of their role under varying climatic conditions. Although soil  
244 textural properties have been shown to drive the soil moisture variability at hyper-resolutions (Vegropolan et al.,  
245 2022), the vertical and seasonal influence on these properties in soil moisture simulation at this scale remains  
246 unknown. Hence, a Sobol sensitivity analysis (Sobol, 1993) is performed on the soil parameters of HydroBlocks  
247 (parameters used in Noah-MP) at the HRU scale and at every timestep. Eight soil parameters are considered,  
248 which include the Brooks-Corey parameter (BB), wilting point (WLTSMC), porosity (MAXSMC), field capacity  
249 (REFSMC), soil moisture limiting direct evaporation (DRYSMC), saturation soil matric potential (SATPSI),  
250 saturated hydraulic conductivity (SATDK) and saturated soil-water diffusivity (SATDW). To minimize the  
251 computational time, we selected a small watershed of 402.1 km<sup>2</sup> within the basin to perform the sensitivity test  
252 across all of its HRUs. The watershed is predominantly cropland (96%), waterbodies (2.3%), and with the  
253 remainder 1.7% for urban and mixed forest. The watershed has flat terrain with elevation range between 376m  
254 and 548m and clay content (30% to 42.6%). To assess the sensitivity of soil parameters with respect to depth,  
255 Sobol analysis is carried out on soil moisture simulations obtained from HydroBlocks VHet version at each soil  
256 layer and each timestep across all HRUs in the selected watershed. We considered a variability of one standard  
257 deviation for each soil parameter in the sensitivity analysis. The Sobol analysis is carried out using the Python  
258 package SALib (Herman and Usher, 2017). In this test, HRUs under urban land cover are omitted due to the lack  
259 of information and variability of soil parameters in these regions. This test decomposes the total variance  $V$  of the  
260 model output as a combination of variances of each input parameter as  $V_i$  and as variances of its interactions with  
261 other parameters.

$$262 \quad V = \sum_i V_i + \sum_{i<j} V_{ij} + \sum_{i<j<k} V_{ijk} + V_{12,\dots,n} \quad (1)$$

263  $V_{ij}$  is the variance in the model output corresponding to the interaction between parameters  $i$  and  $j$ , and hence

264  $V_{12,\dots,n}$  represents all the interactions higher than the third order.





265  $S_i$  is the first-order Sobol index representing the contribution of each parameter without considering its interaction  
266 with other parameters. The total contribution from parameter  $i$ , including its interaction with other parameters, is  
267 defined by the total order of Sobol index  $S_{Ti}$ . This can also be written in terms of total variance,  $V$  when the sum  
268 of all variances where every parameter is varied except the parameter  $i$  as  $V_{-i}$ . Hence, the first-order Sobol index  
269  $S_i$  and total-order Sobol index  $S_{Ti}$  are as follows.

$$270 \quad S_i = \frac{V_i}{V}, \quad (2)$$

$$271 \quad S_{Ti} = 1 - V_{-i}/V \quad (3)$$

272 Soil moisture generated from the model is a time series data. Hence, Sobol indices are calculated at each timestep  
273 for all parameters under consideration. Further, following (Cuntz et al., 2016), the  $V_{12,\dots,n}$  arithmetic mean of Sobol  
274 indices is calculated over all time steps as given below. The time series of sensitivity is utilized to assess the role  
275 of seasonality in influencing soil parameter sensitivity on soil moisture profile simulations.

$$276 \quad \bar{S}_i = \frac{1}{T} \sum_{t=1}^T S_i(t) = \frac{1}{T} \sum_{t=1}^T \frac{V_i(t)}{V(t)} \quad (4)$$

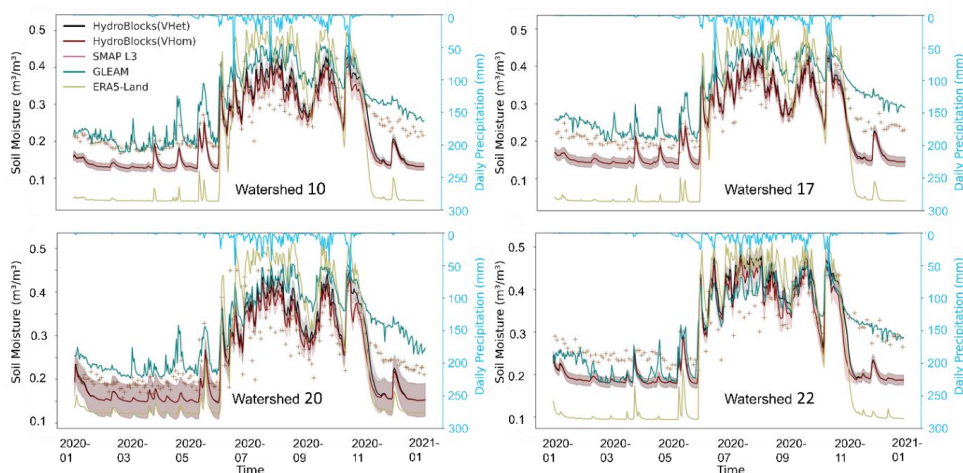
$$277 \quad \bar{S}_{Ti} = \frac{1}{T} \sum_{t=1}^T S_{Ti}(t) = 1 - \frac{1}{T} \sum_{t=1}^T \frac{V_{-i}(t)}{V(t)} \quad (5)$$

### 278 3. Results and Discussion

#### 279 3.1 The capabilities of hyper-resolution simulations for characterizing the soil moisture dynamics

##### 280 3.1.1 Temporal dynamics of surface soil moisture

281 Fig.3 shows the temporal variation of surface soil moisture of different products: HydroBlocks VHet and VHom,  
282 SMAP L3, GLEAM, and ERA5-Land for four watersheds. The HydroBlocks model configurations (VHet and  
283 VHom) are shown at a location corresponding to an SMAP grid. During dry seasons (October to May), the soil  
284 moisture spatial variability of HydroBlocks simulations are consistent, as shown in terms of its standard deviation  
285 in shades. From all the data products, only ERA5-Land is drier than HydroBlocks simulations in the dry period.  
286 During the monsoon season, HydroBlocks simulations showed less spatial variability (black and maroon shades  
287 in Fig.3); however, less consistency than during the dry periods. Considering that the only difference between the  
288 two HydroBlocks model configurations is the vertical heterogeneity of subsurface soil layers, the observable  
289 differences in surface soil moisture during the monsoon can be attributed to the influence of soil properties at the  
290 deeper layers, especially during active wetting/drying conditions. Compared to other data products, ERA5-Land  
291 exhibits sudden wetups with increased precipitation towards the onset of the monsoon and steeper drydown as the  
292 monsoon recedes. During monsoon, ERA5-Land shows high wet bias compared to other data products. Despite  
293 using the same meteorological forcing as ERA5-Land, HydroBlocks simulations were more consistent and able  
294 to better represent the temporal dynamics of SMAP L3 surface soil moisture. There are several differences  
295 between the HydroBlocks and ERA5-Land in terms of soil hydrology processes (e.g., accounting for lateral  
296 connectivity), modeling resolution, parameterizations, and supporting datasets. ERA5-Land defines soil  
297 properties based on soil texture information derived from soil depth (30-100 cm) of FAO Digital Soil Map of  
298 World at 9 km resolution (Muñoz-Sabater et al., 2021). This soil data ignores horizontal and vertical spatial  
299 variability of soil properties at the field scale in the study region (Dai et al., 2019; Poggio et al., 2021). Further,  
300 HydroBlocks used in this study do not account for surface channel routing, whereas ERA5-land does, which can  
301 also influence soil moisture variations.



302

303 **Figure 3:** Time series of surface soil moisture simulations from HydroBlocks (VHet and VHom configurations)  
304 compared with SMAP L3, ERA5-Land, GLEAM surface soil moisture ( $\text{m}^3\text{m}^{-3}$ ), and ERA5-Land daily  
305 precipitation (mm). Soil moisture values considered from all datasets for the year 2020 correspond to a randomly  
306 identified SMAP L3 grid in each of the four watersheds. Both HydroBlocks simulations are represented by the  
307 mean soil moisture from all 30 m grids within the SMAP L3 grid, with one spatial standard deviation shown as a  
308 light-coloured band around the mean.

309 During the dry season (October to May), HydroBlocks VHom and VHet surface soil moisture simulations are  
310 consistent with SMAP L3 observations with the exception of dry bias of  $-0.056 \text{ m}^3\text{m}^{-3}$  and  $-0.051 \text{ m}^3\text{m}^{-3}$ ,  
311 respectively. Conversely, during the monsoon, HydroBlocks simulations have a wet bias of  $0.015 \text{ m}^3\text{m}^{-3}$  and  $0.032$   
312  $\text{m}^3\text{m}^{-3}$  compared to SMAP L3. However, during saturated conditions, where soil moisture is around  $0.45 \text{ m}^3\text{m}^{-3}$ ,  
313 there is a convergence between HydroBlocks VHet and VHom simulations and SMAP soil moisture. In  
314 HydroBlocks, the saturated soil moisture conditions are limited by soil porosity, which is computed through PTFs.  
315 Consistency with satellite observed saturation levels confirms that properties computed using digital soil maps  
316 and PTFs can improve soil moisture modeling performance than those obtained from the look-up table, as also  
317 shown in (Xu et al., 2023).

318 HydroBlocks surface soil moisture simulation, compared to that of GLEAM data at  $0.25^\circ$  spatial resolution, shows  
319 minimal temporal variability with steeper drydown towards the end of the monsoon. HydroBlocks represents  
320 surface soil moisture at 5 cm depth and uses Richards equations in Noah-MP to account for the vertical flow of  
321 soil water. In contrast, GLEAM represents soil moisture for a 10 cm profile and uses a simplified drainage scheme  
322 independent of soil properties except for wilting point and soil porosity (Martens et al., 2017). This simplification  
323 is beneficial for enhancing computational efficiency (Martens et al., 2017); however, it ignores various subgrid  
324 processes and is hence not suitable for field-scale application.

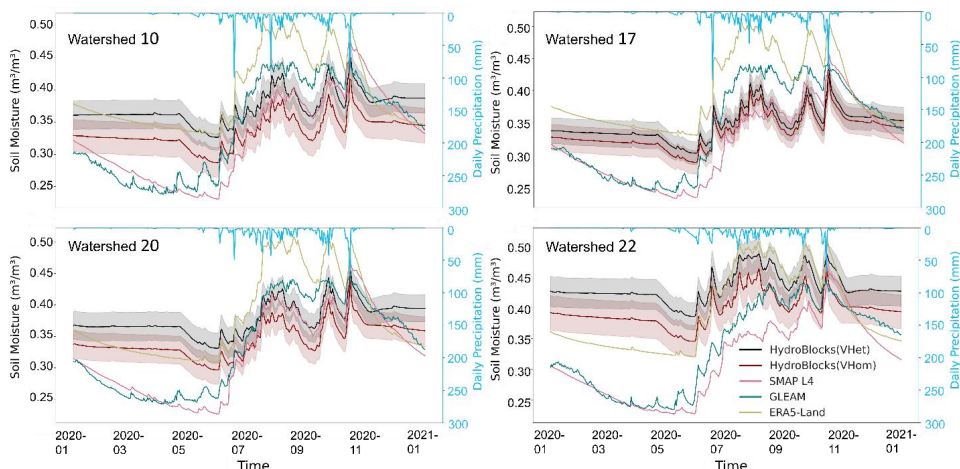
### 325 3.1.2 Temporal dynamics of rootzone soil moisture

326 Fig.4 shows the temporal variation of rootzone soil moisture (1 meter deep) for different products, including two  
327 HydroBlocks model configurations at a location corresponding to an SMAP pixel in four different watersheds.  
328 Results show a wet bias of  $0.03 \text{ m}^3\text{m}^{-3}$  between HydroBlocks (VHet) and HydroBlocks (VHom). During the dry



329 period from January to May, neither model configuration depicts a noticeable drydown except for later months in  
330 the period. Precipitation events were limited and of low magnitude, causing low evaporation. However, other soil  
331 moisture data products show a consistent drydown pattern throughout the period. HydroBlocks simulations do not  
332 depict a prominent drydown since the monthly LAI values are zero from the Noah-MP parameter table,  
333 MPTABLE.TBL, thus, indicates no transpiration till April. Towards the end of April, as LAI increases,  
334 transpiration also increases, causing a discernible drydown pattern in both HydroBlocks configurations. To  
335 address this limitation, we expect that incorporating dynamic LAI as an input in Noah-MP parameterization  
336 improves vegetation accountability and transpiration estimation. However, implanting dynamic vegetation in  
337 hyper-resolution scales increases the complexity and is beyond the purview of current work. Such a modification  
338 shall be included in future versions of the model.

339 During the monsoon, with the increase in precipitation events and their intensities, soil moisture variability  
340 increases in all data products. HydroBlocks VHet and VHom rootzone soil moisture values were consistent with  
341 SMAP L4 and GLEAM; however, they showed a significant dry bias of  $-0.056 \text{ m}^3\text{m}^{-3}$  and  $0.08 \text{ m}^3\text{m}^{-3}$  compared  
342 to ERA5-Land during the monsoon. Unlike HydroBlocks rootzone soil moisture, which saturates at  $0.4 \text{ m}^3\text{m}^{-3}$ ,  
343 ERA5-Land data saturates at  $0.5 \text{ m}^3\text{m}^{-3}$  in monsoon.



344 **Figure 4:** Time series plots of rootzone soil moisture simulations from HydroBlocks (VHet and VHom  
345 configurations) compared with SMAP L4, ERA5-Land, GLEAM rootzone soil moisture ( $\text{m}^3\text{m}^{-3}$ ), and ERA5-Land  
346 daily precipitation (mm). Soil moisture values considered from all datasets for the year 2020 corresponded to a  
347 randomly identified SMAP L4 pixel in each of the four watersheds. HydroBlocks rootzone soil moisture  
348 simulations are represented by the mean soil moisture from all 30 m grids within the SMAP L4 pixel, with one  
349 standard deviation shown as a light-colored band around the mean.  
350

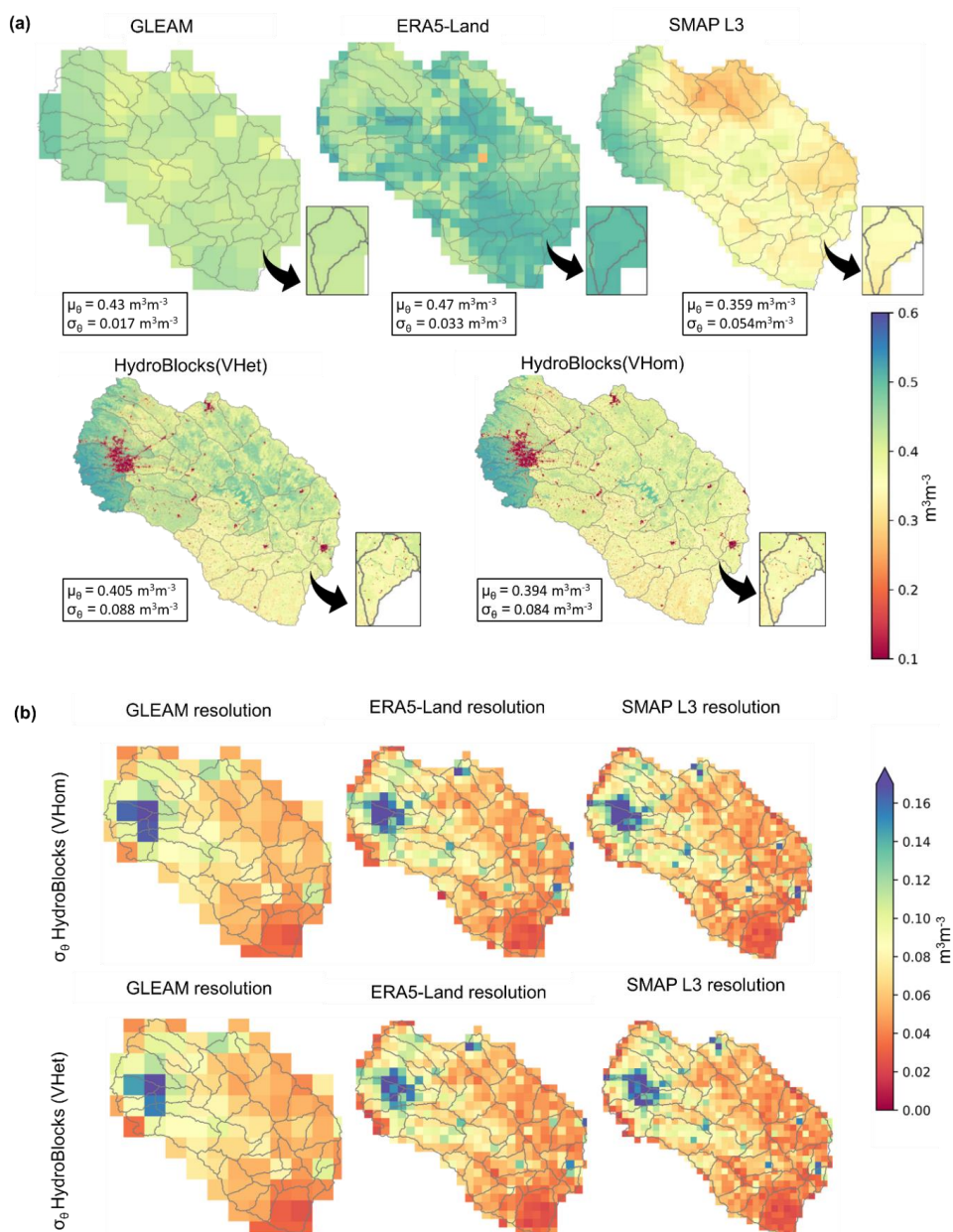
### 351 3.1.3 Spatial dynamics of surface soil moisture

352 The spatial distribution of surface soil moisture estimates for GLEAM, ERA5-Land, SMAP L3, and HydroBlocks  
353 (VHom and VHet) are shown in Fig. 5(a). HydroBlocks and SMAP L3 soil moisture data show a transition from  
354 wetter in the west to drier soil conditions in the east, reflecting the spatial pattern of precipitation across the basin.  
355 Compared to HydroBlocks simulations, SMAP L3 soil moisture data shows a smoother transition, which can be



356 attributed to the effect of interpolation of original SMAP retrieval at 36 km to 9km (Chaubell et al., 2016). As  
357 expected, the HydroBlocks surface soil moisture shows substantial spatial variability (represented by the spatial  
358 standard deviation  $\sigma_0$ , of  $V_{Het} = 0.088 \text{ m}^3\text{m}^{-3}$  and  $V_{Hom} = 0.084 \text{ m}^3\text{m}^{-3}$ ) compared to macroscale products ( $\sigma_0$  of  
359 SMAP L3 =  $0.054 \text{ m}^3\text{m}^{-3}$ , ERA5-Land =  $0.033 \text{ m}^3\text{m}^{-3}$ , and GLEAM =  $0.017 \text{ m}^3\text{m}^{-3}$ ). The spatial variability of  
360 HydroBlocks surface soil moisture is shown for each coarse resolution pixel corresponding to the coarser scale  
361 products in Fig.5(b). The dry soil conditions in urban areas of some watersheds result in high soil moisture  
362 variability with a spatial standard deviation exceeding  $0.16 \text{ m}^3\text{m}^{-3}$  at all the macroscale product resolutions.  
363 However, this behavior is likely a response to how urban areas are parametrized in the model rather than only the  
364 soil hydrologic process. Further, drier watersheds in the south exhibit a low standard deviation ( $\sim 0.02 \text{ m}^3\text{m}^{-3}$ ) in  
365 this region.

366 At a watershed scale, represented by the inset of Fig.5(a), we can observe higher spatial heterogeneity in  
367 HydroBlocks  $V_{Het}$  and  $V_{Hom}$  simulations than in SMAP L3, ERA5-Land, and GLEAM soil moisture data.  
368 HydroBlocks simulations in this watershed, although spatially consistent with SMAP L3 observations, reveal a  
369 detailed variation. We can observe wet soil patches near streams or dry soil in higher elevations to the south of  
370 this watershed. Similar spatial heterogeneity is not observed in the estimates of other datasets because of their  
371 coarse resolution. Besides, this watershed has a spatial extent less than GLEAM's  $0.25^\circ$  grid resolution.  
372 Improvement in spatial variability at a localized scale is a response to the combined interactions between the  
373 meteorological forcing, topography, land cover types, and soil properties (Vergopolan et al., 2022).

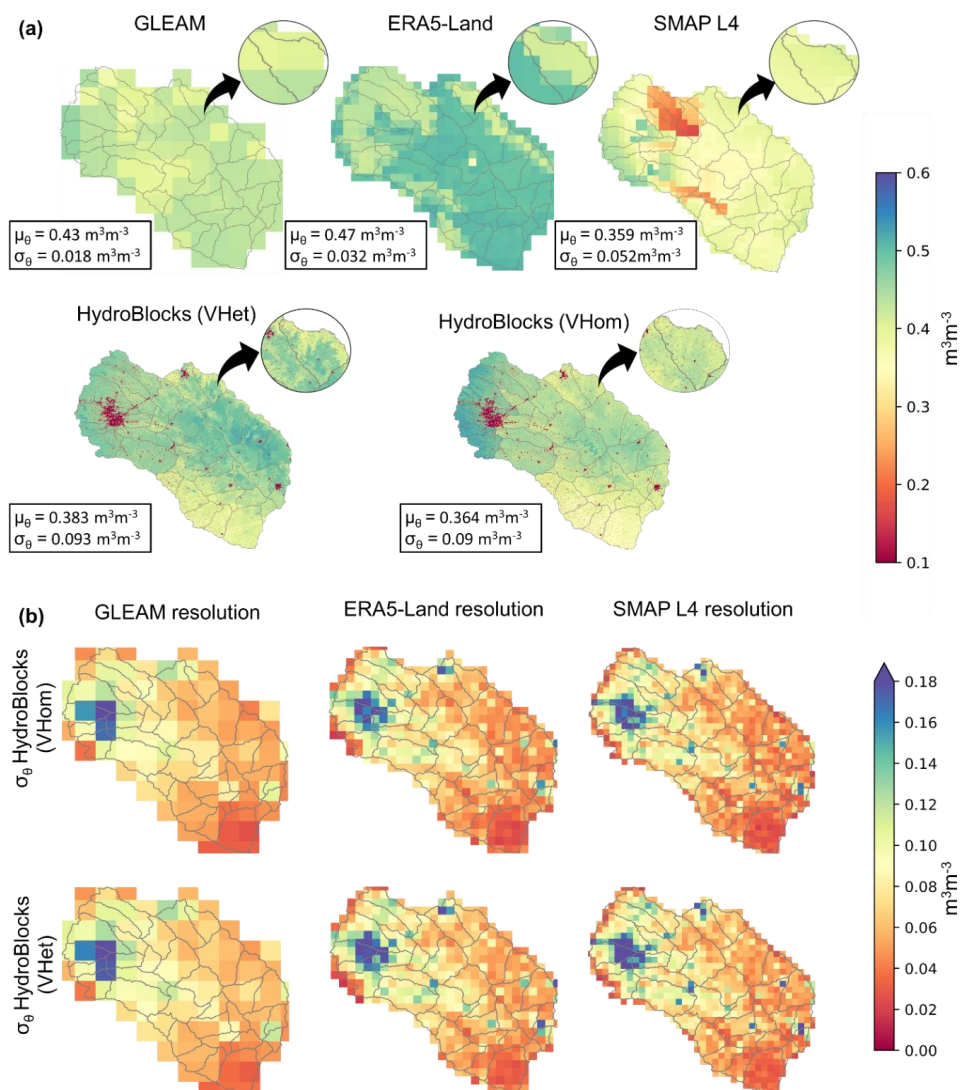


374  
 375 **Figure 5:** (a) The spatial maps of surface soil moisture on August 6, 2020, were obtained from HydroBlocks  
 376 simulations compared with ERA5-Land, GLEAM, and SMAP L3 data. The soil moisture mean ( $\mu_\theta$ ) and spatial  
 377 standard deviation ( $\sigma_\theta$ ) of the entire basin for each data product are also shown. The inset shows the simulations  
 378 at a watershed scale (watershed 20 with an area of 402 km<sup>2</sup>). (b) Spatial standard deviations ( $\sigma_\theta$ ) of HydroBlocks  
 379 (VHet and VHom configurations) surface soil moisture (at 30 m resolution) estimates within coarser resolution  
 380 pixels of different macroscale products.



381 **3.1.4 Spatial dynamics of rootzone soil moisture**

382 Fig.6(a) shows the spatial maps of the rootzone soil moisture estimates on August 6, 2020, across the whole basin  
383 from GLEAM, ERA5-Land, SMAP L4, and HydroBlocks VHet and VHom. As for the surface, HydroBlocks  
384 rootzone soil moisture shows higher spatial variability ( $\sigma_0$  of VHet =  $0.093 \text{ m}^3\text{m}^{-3}$  and VHom =  $0.09 \text{ m}^3\text{m}^{-3}$ ) than  
385 other macroscale products ( $\sigma_0$  of SMAP L3 =  $0.052 \text{ m}^3\text{m}^{-3}$ , ERA5-Land =  $0.032 \text{ m}^3\text{m}^{-3}$ , and GLEAM =  $0.018$   
386  $\text{m}^3\text{m}^{-3}$ ). However, the rootzone variability is higher than the surface soil moisture variability. HydroBlocks  
387 simulations show wet soil in most of the basin, except for watersheds 11, 12, 13, and 19 in the south, where soil  
388 is dry. The spatial pattern of HydroBlocks simulations is not consistent with any of the macroscale data at a basin  
389 scale. However, at a regional scale, soil moisture simulations from HydroBlocks and other products show  
390 similarities, although HydroBlocks simulations demonstrate high spatial variability. For example, in Watersheds  
391 5, 6, 7, and 8, simulations of HydroBlocks (both configurations) and ERA5-Land show the influence of  
392 topography where the soil is drier at the ridges and wet in the foothills. However, HydroBlocks simulation shows  
393 better spatial variability, which is evident from its spatial standard deviation within the corresponding ERA5-Land  
394 grid cells (Fig.6(b)). Watersheds 23, 29, and 31 towards the west of the basin receive high precipitation and have  
395 numerous tributaries, causing the soil to be wet with more spatial variability in HydroBlocks simulations than  
396 SMAP L4 data. Figure 6(b) shows the spatial standard deviation of rootzone soil moisture simulated by  
397 HydroBlocks (VHom) and HydroBlocks (VHet) for each coarser resolution pixel of the macroscale products.  
398 HydroBlocks could simulate the dryness in soil moisture in the urban area, causing a high standard deviation ( $\sim 0.2$   
399  $\text{m}^3\text{m}^{-3}$ ) within the corresponding coarse resolution grid cells. Macroscale products like GLEAM have wide  
400 applicability in hydroclimatic studies (Baker et al., 2021), particularly due to their improved accuracy in  
401 estimating evapotranspiration (Ding and Zhu, 2022; Zhu et al., 2022). However, macroscale products overlook  
402 the sub-grid scale process, including lateral connectivity and heterogeneity in land cover types at the field scale  
403 (Wood et al., 2011). Agricultural applications require spatial heterogeneity of rootzone soil moisture at the field  
404 scale (Vergopolan et al., 2021).



405

406 **Figure 6:** (a) The spatial maps of rootzone soil moisture on August 6, 2020, were obtained from HydroBlocks  
 407 simulations compared with ERA5-Land, GLEAM, and SMAP L4 data. The soil moisture mean (μ<sub>θ</sub>) and spatial  
 408 standard deviation (σ<sub>θ</sub>) of the entire basin for each data product are also shown. The insets reveal the spatial details  
 409 of the simulations at a local scale. (b) Spatial standard deviations (σ<sub>θ</sub>) of HydroBlocks (VHet and VHom  
 410 configurations) rootzone soil moisture (at 30 m resolution) estimates within coarser resolution pixels of different  
 411 macroscale products.

412 Further comparing the two model configurations, HydroBlocks (VHet) simulations show soil to be wet in plain  
 413 topography and drier in hilly areas to the west of the basin than HydroBlocks (VHom) simulations. At field scale,  
 414 HydroBlocks (VHet) offers higher spatial variability than HydroBlocks (VHom) in both surface and rootzone soil  
 415 moisture simulations. A farm-scale soil moisture simulation with improved sub-grid variability is valuable for



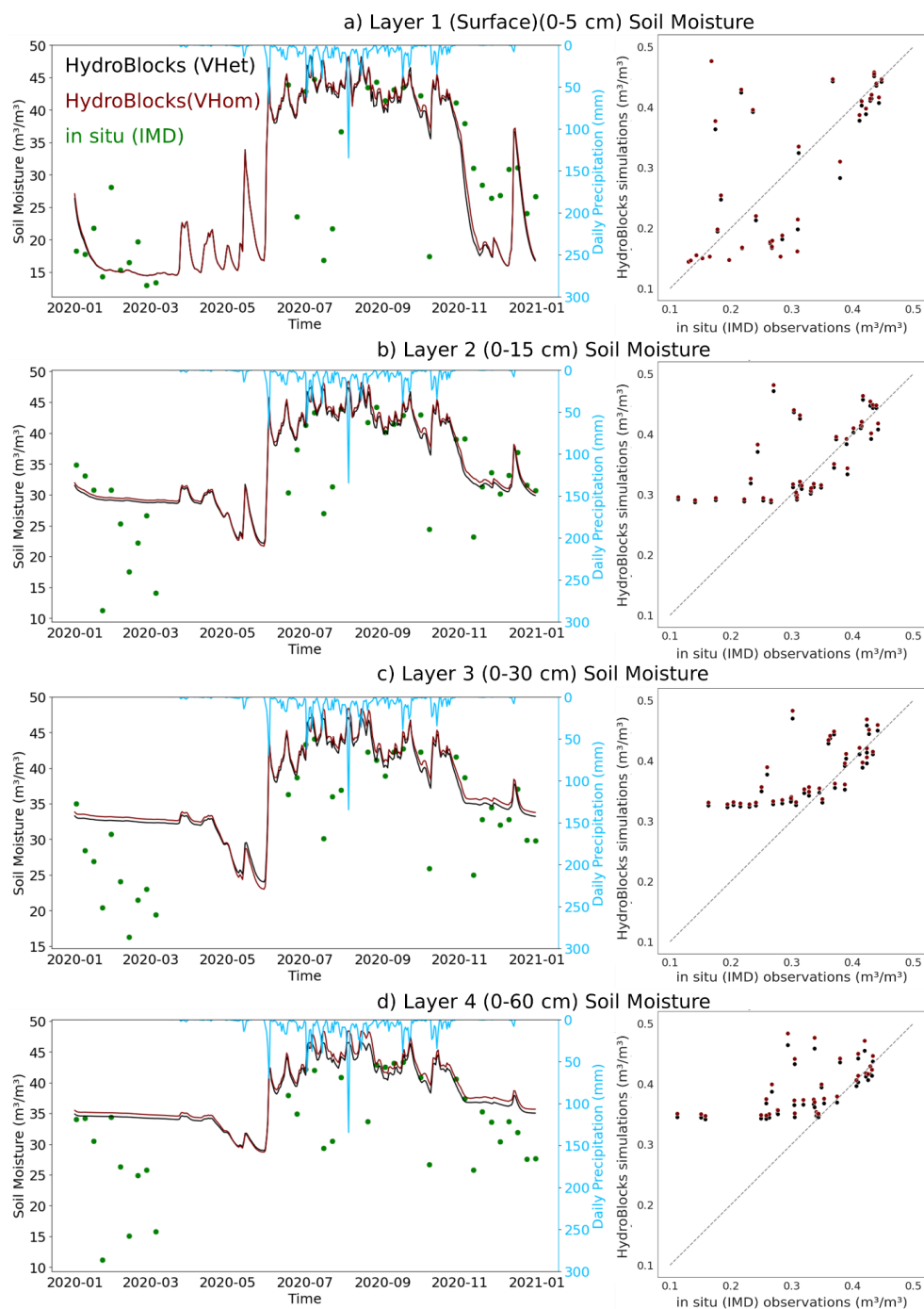
416 precision irrigation and water resources management (Peng et al., 2021). Root zone soil moisture indicates water  
417 availability to plants, and its spatial variability significantly impacts crop yield and their predictions (Holzman et  
418 al., 2014). However, both model configurations of HydroBlocks could simulate soil moisture with higher spatial  
419 variability than in macroscale products. We further evaluated the performance of HydroBlocks, and the results  
420 are discussed in the next section.

### 421 **3.2 Model Performance**

#### 422 **3.2.1. Validation with IMD in-situ observations**

423 In-situ monitoring of soil moisture is a challenge in agriculture dominant countries like India, which have  
424 fragmented farming systems (Karthikeyan and Kumar, 2016; Vergopalan et al., 2021). In view of these  
425 limitations, we could validate HydroBlocks VHet and VHom simulations with in-situ soil moisture data at only  
426 one location. Fig.7 presents the timeseries and scatterplots of VHet and VHom simulations of an HRU  
427 corresponding to location where in-situ station is situated in watershed 29. Fig. 7(a) corresponds to the surface  
428 layer (0-5 cm), Fig. 7(b) corresponds to layer 2 (0-15 cm), Fig. 7(c) corresponds to layer 3 (0-30 cm) and Fig 4  
429 corresponds to layer 4 (0-60 cm) ; Table 2 presents the layer-wise performance VHet and VHom simulations. In  
430 the case of surface soil moisture, results reveal that both HydroBlocks configurations exhibited similar  
431 performance. Both VHet and VHom configurations have low bias ( $-0.001 \text{ m}^3\text{m}^{-3}$   $0.003 \text{ m}^3\text{m}^{-3}$ ) with similar  
432 ubRMSE ( $0.096 \text{ m}^3\text{m}^{-3}$  and  $0.097 \text{ m}^3\text{m}^{-3}$ ) and correlation ( $R = 0.66; 0.66$  and  $R_{sp} = 0.66; 0.67$ ) when compared to  
433 in-situ observations.





434

435 **Figure 7:** Time series of HydroBlocks (VHet and VHom configurations) simulations of soil moisture at different  
 436 layers ((a) 0-5 cm (surface), (b) 0-15 cm, (c) 0-30 cm, (d) 0-60 cm with ERA5-Land daily precipitation (mm),



437 which is used as the forcing in the model, are compared with IMD in situ soil moisture observations at watershed  
 438 29. Scatterplots comparing the HydroBlocks simulations and in situ observations are also included beside  
 439 layerwise soil moisture time series. HydroBlocks simulations are converted to daily timescale before comparing  
 440 against insitu observations.

441 **Table 2.** Performance metrics of layer wise simulations of HydroBlocks VHet and VHom configurations against  
 442 IMD in situ observations.

	Layer 1 (Surface (0-5 cm))		Layer 2 (0-15 cm)		Layer 3 (0-30 cm)		Layer 4 (0-60 cm)	
	VHom	VHet	VHom	VHet	VHom	VHet	VHom	VHet
<b>Bias</b> ( $\text{m}^3\text{m}^{-3}$ )	0.003	-0.001	0.036	0.030	0.051	0.044	0.067	0.059
<b>ubRMSE</b> ( $\text{m}^3\text{m}^{-3}$ )	0.096	0.097	0.067	0.067	0.055	0.055	0.066	0.066
<b>R</b>	0.66	0.66	0.63	0.63	0.70	0.70	0.59	0.60
<b>R<sub>sp</sub></b>	0.67	0.66	0.67	0.67	0.80	0.80	0.67	0.68

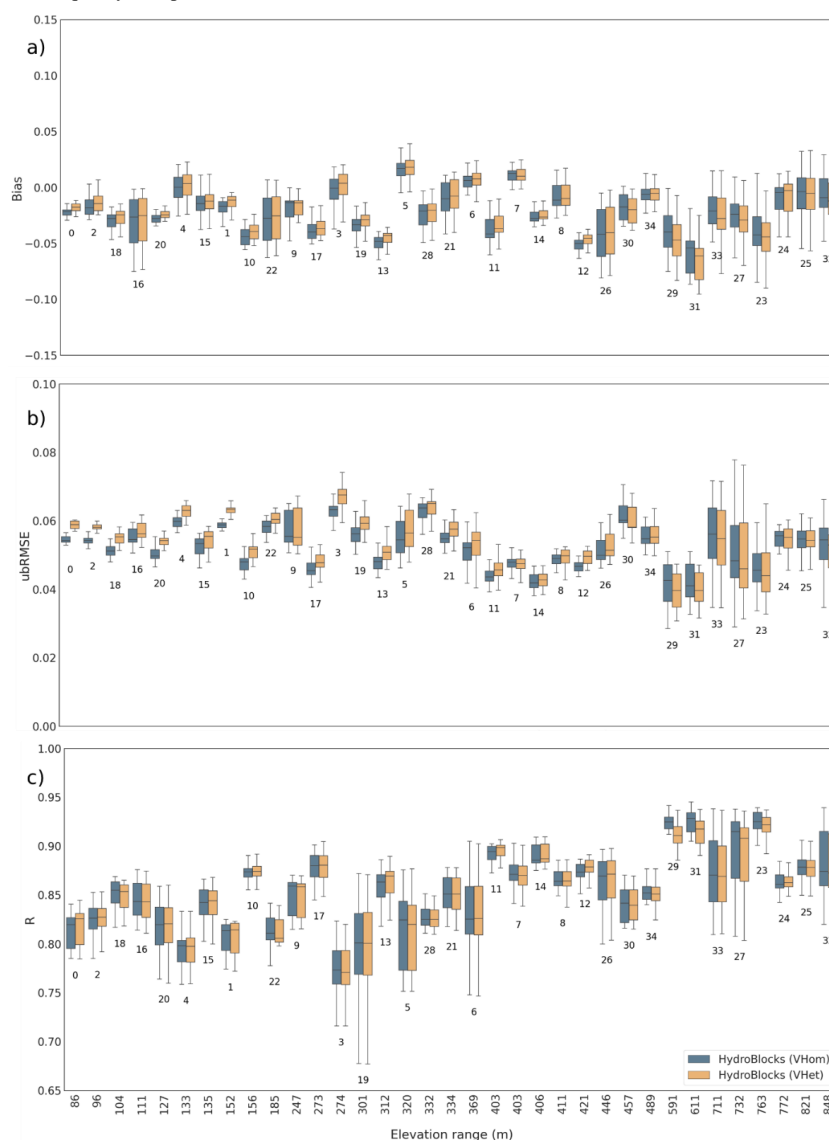
443  
 444 In the case of subsurface layers, soil moisture simulations from VHet slightly outperformed VHom, particularly  
 445 by reducing the bias. In all the sub surface soil layers at different depths (0-15 cm ,0-30 cm, 0-60 cm), VHet  
 446 simulations show lower bias ( $0.030 \text{ m}^3\text{m}^{-3}$ ,  $0.044 \text{ m}^3\text{m}^{-3}$  and  $0.059 \text{ m}^3\text{m}^{-3}$ ) than VHom ( $0.036 \text{ m}^3\text{m}^{-3}$ ,  $0.051 \text{ m}^3\text{m}^{-3}$   
 447  $^3$  and  $0.067 \text{ m}^3\text{m}^{-3}$ ). However, there is no change in ubRMSE values ( $\sim 0.067 \text{ m}^3\text{m}^{-3}$ ,  $0.055 \text{ m}^3\text{m}^{-3}$ , and  $0.066 \text{ m}^3\text{m}^{-3}$ ).  
 448  $^3$ ). This indicates that incorporating soil vertical properties into the model has brought a systematic improvement  
 449 (thus, the difference in bias) in deeper layers. VHet configuration also show a marginal improvement in the  
 450 correlation values in the deeper layer ( at depth 0-60cm) with R and R<sub>sp</sub> (0.60 and 0.68) than VHom's values (0.59  
 451 and 0.67, respectively) at the site. Both VHet and VHom configurations show similar correlation values in other  
 452 sub surface layers – R = 0.67 and R<sub>sp</sub> = 0.67 for layer (0-15 cm) and R = 0.7;R<sub>sp</sub> = 0.80 for layer (0-30 cm). VHet  
 453 simulations have shown good agreement with in situ soil moisture during the monsoon season (Fig. 7 (b,c,d)).  
 454 Furthermore, the wetup and drydown patterns of both configurations are largely consistent with in situ  
 455 observations and precipitation. It is important to note that there could be uncertainties due to the lack of dense  
 456 network of observations, which can affect the performance (Chen et al., 2017). Despite uncertainties, VHet  
 457 followed by VHom simulations are reasonably accurate when compared to the ground truth. To gain further  
 458 confidence on the quality of simulations and account for land surface heterogeneity, we evaluated the model  
 459 simulations against SMAP L3 and SMAP L4 soil moisture data and discussed in Sect 3.2.2.

### 460 3.2.2 Comparison with SMAP L3 and L4 soil moisture data

461 The boxplots shown in Fig. 8 explain the quality of HydroBlocks VHet and VHom surface soil moisture  
 462 simulations with respect to SMAP L3 observations. Only those SMAP L3 pixels that have recommended retrieval  
 463 quality are considered during this analysis. Performance is assessed using bias, ubRMSE, and Pearson correlation.  
 464 Most of the watersheds have a dry bias compared to SMAP L3. Exceptions are there, with some watersheds having  
 465 a marginal wet bias, however, less than  $0.025 \text{ m}^3\text{m}^{-3}$ . The average median bias values, across the basin, for



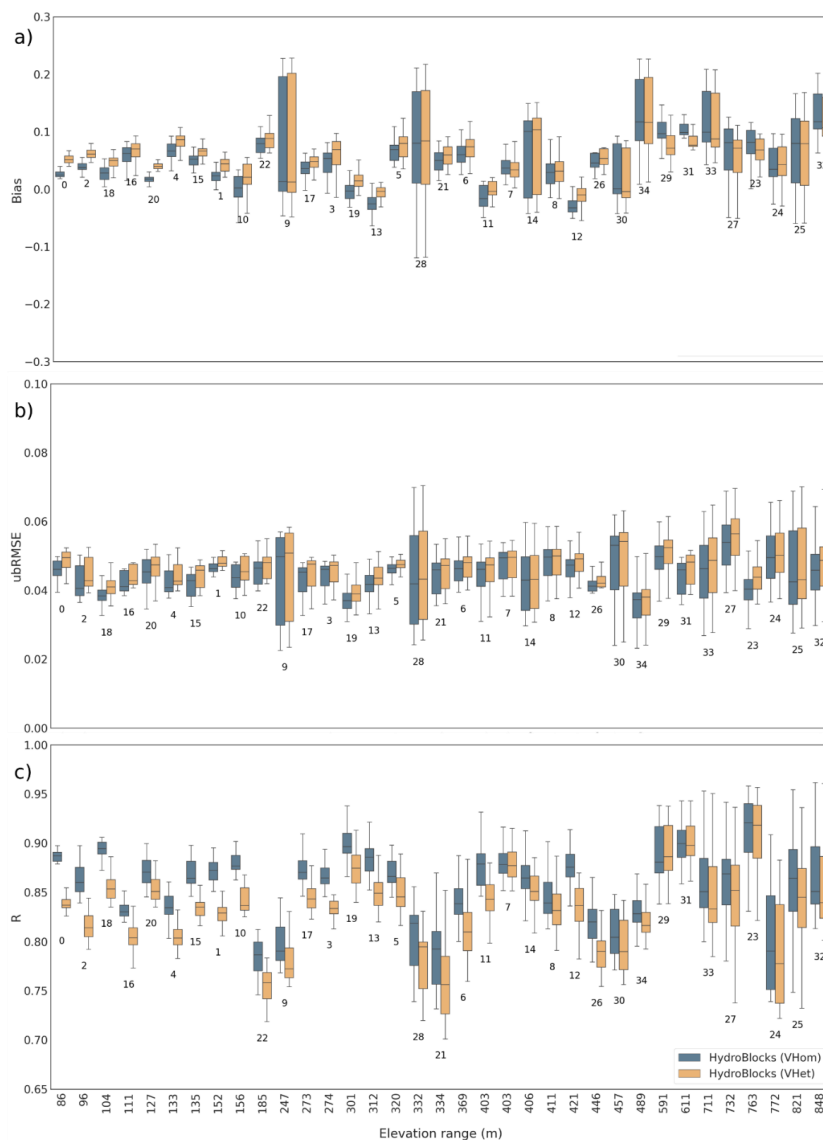
466 HydroBlocks VHet and VHom simulations are  $-0.02 \text{ m}^3\text{m}^{-3}$  and  $-0.021 \text{ m}^3\text{m}^{-3}$ , respectively. There is no clear trend  
 467 or pattern in the bias values of watersheds following their elevation range. However, watersheds with higher  
 468 relative relief, greater than 500m, show higher variability marked by long whiskers than other watersheds. Further  
 469 watersheds with low variation in bias are more commonly found in regions with smaller elevation ranges.  
 470 Although exceptions exist in both cases, a possible reason is that some of these watersheds (e.g., 22, 27, 29, and  
 471 31) have a significant portion of their area urban or waterbodies, causing fewer SMAP L3 pixels with  
 472 recommended quality to represent the watershed.



473  
 474 **Figure 8:** Box plot showing the performance of HydroBlocks (VHom) and HydroBlocks (VHet) model in  
 475 simulating surface soil moisture to SMAP L3 observations in terms of (a) bias, (b) ubRMSE, (c) R. Watersheds



476 are arranged in terms of their elevation range (representing topographic variations) along the x-axis. Each boxplot  
477 corresponds to a watershed identified by their number provided in Fig.1.  
478 The ubRMSE median values of HydroBlocks (both configurations) simulated surface soil moisture measurements  
479 vary between  $0.04 \text{ m}^3\text{m}^{-3}$  and  $0.06 \text{ m}^3\text{m}^{-3}$  across 35 watersheds. The median ubRMSE values for HydroBlocks  
480 surface soil moisture simulations are generally higher in the VHet configuration, with a basin-wide average of  
481  $0.053 \text{ m}^3\text{m}^{-3}$  compared to  $0.052 \text{ m}^3\text{m}^{-3}$  for VHom simulations. Further, surface soil moisture simulations from  
482 both model configurations of HydroBlocks also show a strong correlation with SMAP L3 observations, as shown  
483 in Fig.8. Both HydroBlocks configurations have similar median values of Pearson correlation in all  
484 watersheds, with their values lying between 0.78 and 0.95. When upscaled to  $9\text{km} \times 9\text{km}$ , both versions of  
485 HydroBlocks performed well with low bias and high correlation with respect to SMAP L3 observations. Since  
486 both HydroBlocks use the same soil properties at the surface, the difference between their simulation for the  
487 surface layer is minimal. Besides, the influence of soil properties is significant in soil moisture simulations at a  
488 finer scale than at a coarser resolution (Crow et al., 2012).  
489 Further, rootzone soil moisture simulated by HydroBlocks (both model configurations) is compared with SMAP  
490 L4 data for the year 2020 across all SMAP pixels in terms of bias, ubRMSE, and Pearson correlation, and the  
491 results are shown in Fig.9. Contrary to surface soil moisture plots, there is significant wet bias in many watersheds  
492 when compared to SMAP L4 analysis product. The median bias values range between  $-0.01 \text{ m}^3\text{m}^{-3}$  to  $0.15 \text{ m}^3\text{m}^{-3}$   
493 in both HydroBlocks configurations, as shown in Fig.9(a). Most watersheds show minimal variability in ubRMSE  
494 values, ranging from 0.03 to  $0.055 \text{ m}^3\text{m}^{-3}$ , with a few exceptions (watersheds 9, 25, 28, 30 and 33). However, the  
495 median ubRMSE values across all watersheds remain below  $0.055 \text{ m}^3\text{m}^{-3}$  (see Fig. 9(b)) and have a higher  
496 correlation with SMAP L4 data, with their median Pearson correlation values ranging between 0.76 and 0.93, as  
497 shown in Fig 8(c). The median correlation values for VHom simulations are marginally higher, with an average  
498 of 0.85, while VHet simulations have an average median correlation value of 0.83. The higher correlation of  
499 VHom simulations to SMAP L4 data can also be due to vertically homogeneous soil parameters considered in the  
500 CLM while generating SMAP L4 rootzone soil moisture data. However, in either configurations, performance  
501 metrics reveal higher consistency between model simulated rootzone soil moisture and SMAP L4 data.



502

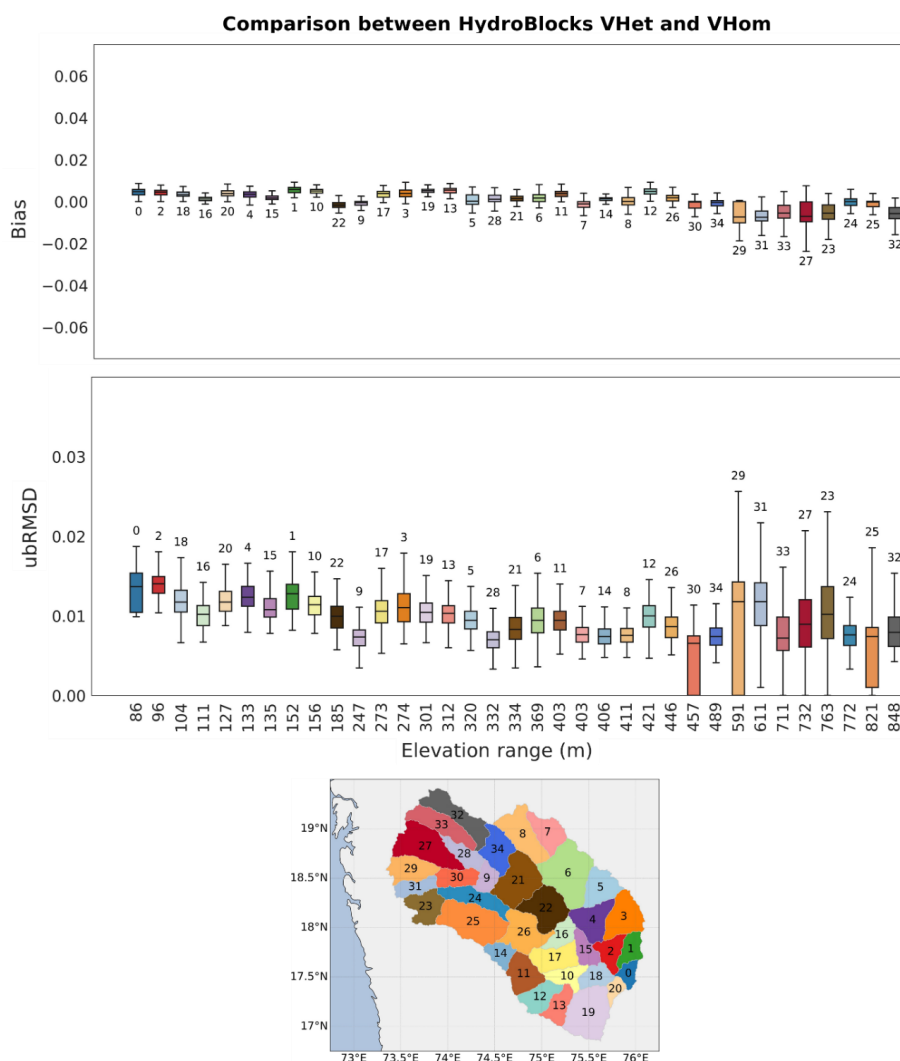
503 **Figure 9:** Box plot showing the performance of HydroBlocks VHom and VHet configurations in simulating  
504 rootzone soil moisture to SMAP L4 observations in terms of (a) bias, (b) ubRMSE, (c) R. Watersheds are arranged  
505 according to their elevation range (representing topographic variations) along the x-axis. Each boxplot  
506 corresponds to a watershed identified by their number near the whiskers, matching those provided in Fig 1.

### 507 3.3 Importance of Soil Vertical Heterogeneity in HydroBlocks

508 We compared layer-wise soil moisture from HydroBlocks VHet and VHom experiments in terms of mean bias  
509 and unbiased Root Mean Square Difference (ubRMSD). Such a comparison is done to understand the changes in  
510 the model simulations after incorporating soil vertical heterogeneity in the model. Surface soil moisture from both



511 configurations is compared at each HRU for each watershed, as shown in Fig.10. Watersheds are sorted in terms  
512 of their elevation range to check for topographic influence. A low wet bias, with median values close to zero, was  
513 attributed to the same soil properties in the surface soil layer for both configurations. Consequently, no substantial  
514 evidence exists that soil moisture simulations in the surface layer differ according to topographical variations.  
515 The ubRMSD between the two configurations has median values in all watersheds around  $0.01 \text{ m}^3\text{m}^{-3}$  and no  
516 greater than  $0.02 \text{ m}^3\text{m}^{-3}$ . However, in some watersheds, the ubRMSD can reach up to  $0.03 \text{ m}^3\text{m}^{-3}$ . This indicates  
517 that the influence of soil properties is more random at the surface layer (evident from high ubRMSD values) than  
518 having a systematic influence (evident from low bias). It may be noted that Noah-MP follows Richards equation,  
519 which also depends on soil hydraulic properties of adjacent soil layers. Besides, soil parameters in Noah-MP  
520 influence the runoff and infiltration and, eventually, soil moisture (Cuntz et al., 2016; Kishné et al., 2017). In  
521 HydroBlocks (VHet), these soil parameters are heterogeneous along the soil column, and their influence is also  
522 considered in determining the infiltrated water (Niu et al., 2005, 2011).



523

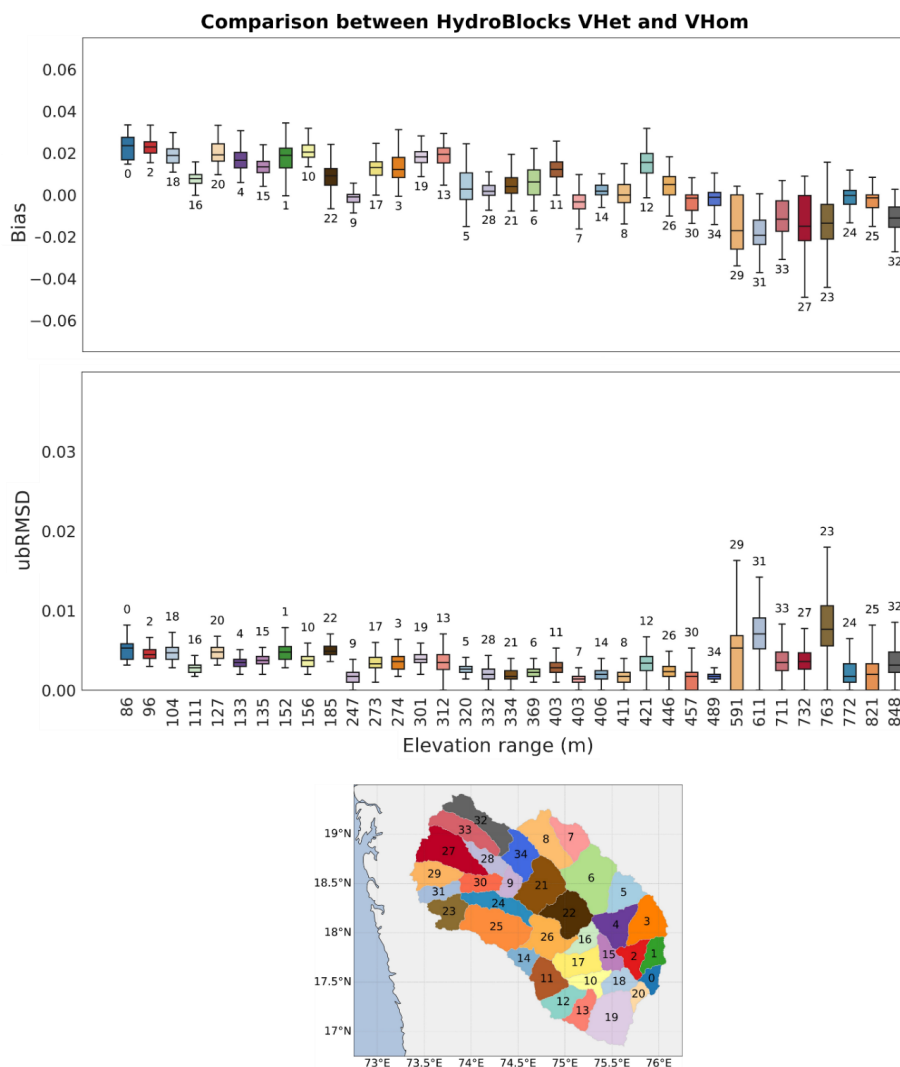
524 **Figure 10:** Box plot showing the comparison between HydroBlocks VHet and VHom configurations in simulating  
 525 surface soil moisture in terms of bias and ubRMSD. These two metrics are calculated for VHet simulations with  
 526 respect to VHom. Watersheds are arranged according to their elevation range (representing topographic  
 527 variations) along the x-axis. Watersheds are identified by their number and colour, as shown in the spatial plot.

528 Figure 11 shows the difference in rootzone soil moisture simulations between HydroBlocks VHet and VHom  
 529 configurations. In the case of rootzone soil moisture, watersheds with less variation in topography (elevation range  
 530  $< 300$  m) show positive bias with their median values around  $0.02 \text{ m}^3\text{m}^{-3}$ , and watersheds having high  
 531 topographical variations tend more to be negatively biased, albeit their median values are close to zero. The  
 532 ubRMSD values between rootzone soil moisture simulations from two model configurations are low, with median  
 533 values less than  $0.01 \text{ m}^3\text{m}^{-3}$ . Exceptions are observed in those watersheds having significant topographic  
 534 variations. However, the ubRMSD values for rootzone soil moisture are lower than surface soil moisture. Indeed,



535 soil moisture simulation variations become more systematic (high bias) in the deeper layers (Fig.S2-S5 in the  
536 Supplementary Material).  
537 There is a transition from wet bias to dry bias in rootzone soil moisture simulations with an increase in topographic  
538 variations, as shown in Fig. 11. Such a transition is not observed when the simulations are compared with SMAP  
539 L4 product at coarse resolution (9 km; Fig. 9). Topography and soil textural properties affect soil moisture  
540 simulations at higher resolution as they are crucial in determining the saturated soil fraction, hence the runoff and  
541 infiltration (Singh et al., 2015). However, in the present study, the difference in both model configurations is only  
542 due to the vertical heterogeneity of soil properties. Hence, any association between rootzone soil moisture and  
543 topographical variation is attributed to soil heterogeneity at subsurface layers and their relationship with  
544 topography. Both soil properties and topographic information influence the subsurface lateral flows. Therefore, it  
545 is crucial to understand the significance of each soil property in simulating soil moisture at each layer. For this  
546 purpose, we performed a sensitivity analysis of Noah-MP soil parameters, which are presented in the next section.





547

548 **Figure 11:** Box plot showing the comparison between HydroBlocks VHet and VHom configurations in simulating  
 549 rootzone soil moisture in terms of bias and ubRMSD. Watersheds are arranged according to their elevation range  
 550 (representing topographic variations) along the x-axis. Watersheds are identified by their number and colour, as  
 551 shown in the spatial plot.

### 552 3.4 Sensitivity Analysis of Soil Parameters

553 We analyzed the results from the Sobol sensitivity test across all the HRUs in watershed 20 to understand the  
 554 most sensitive parameters and their seasonal variation at different layers. Figure 12 presents the sensitivity analysis  
 555 result in one of the HRUs of the watershed within their respective SMAP grid cell (same grid of the time series in  
 556 Fig.3 and Fig.4). Through the Sobol analysis, the role of different parameters and their interactions with each  
 557 other in simulating soil moisture at every layer across the season is studied. The light colour bar represents the



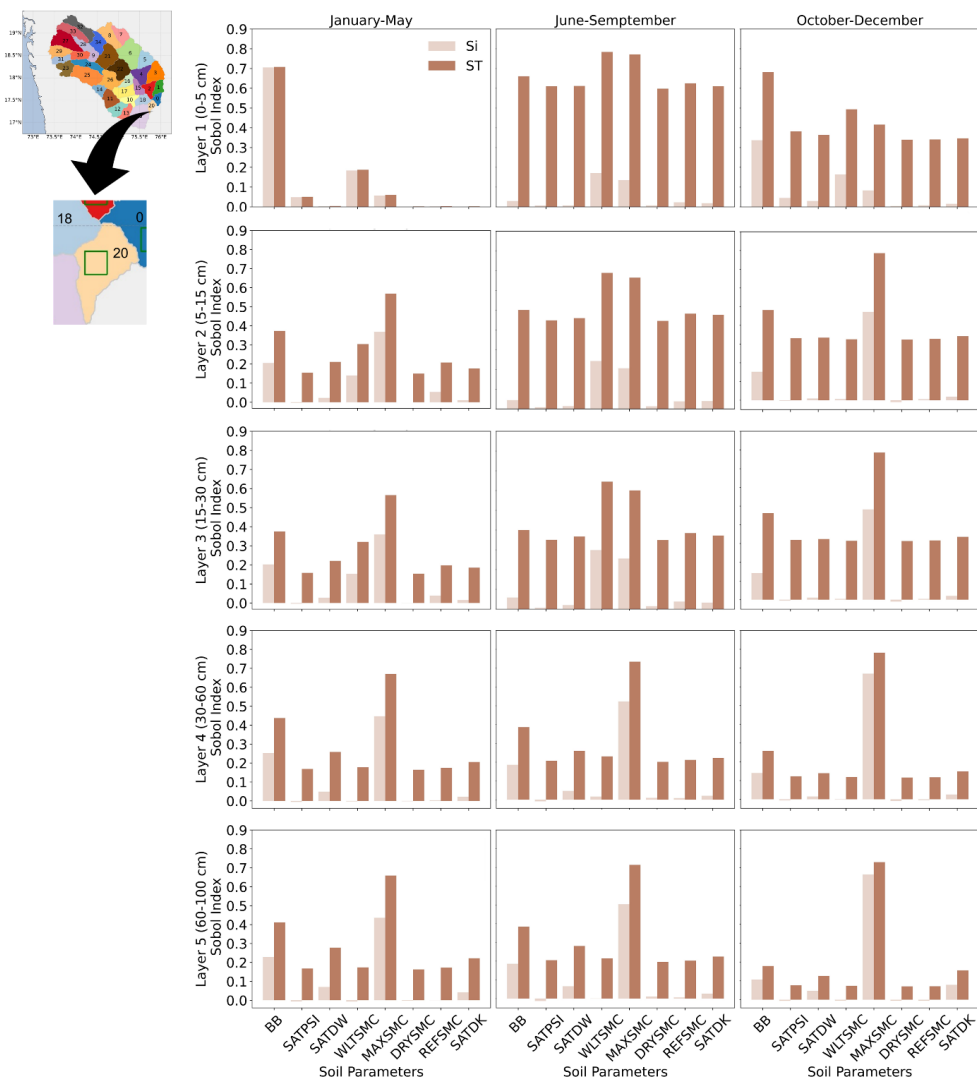
558 first-order Sobol index ( $S_i$ ) value for a parameter indicating the proportion of total variance in soil moisture output,  
559 and it is driven by variance corresponding to only that parameter. The darker colour bar is the total-order Sobol  
560 index ( $S_T$ ), depicting the contribution of that parameter, including its interaction with other parameters, to the total  
561 variance in soil moisture output. Hence, the difference between these two indicates the significance of parameter  
562 interaction.

563 Fig.12 shows that parameter interactions become prominent during the monsoon (June-September), followed by  
564 post-monsoon (October-December), and minimal during the summer months (January-May) at the surface layer.  
565 Although parameter interactions in deeper layers are less than in the surface layer, as expected, these interactions  
566 remain more significant during the monsoon than in other months. This also implies the importance of  
567 precipitation in driving soil hydraulic properties and thus influencing soil moisture dynamics. During the monsoon  
568 (June-September) till layer 3, soil moisture at the wilting point (WLTSMC), soil porosity (MAXSMC), and the  
569 Brooks-Corey parameter (BB) are the significant parameters, while other soil parameters (SATPSI, SATDW,  
570 SATDK, REFSMC, DRYSMC) have equal significance (approximately  $S_T=0.6$  at the surface layer to  $S_T = 0.3$  at  
571 layer 3) as shown in Fig.12. Within the deeper layers (layer 4 and layer 5), the order of parameter significance is  
572 consistent, with MAXSMC as the most significant parameter across all seasons, followed by BB, and the  
573 remaining parameters have equal but less significance. All other parameters have minimal direct significance from  
574 January to May. During the post-monsoon season, interactions increase; however, MAXSMC and BB remain the  
575 only parameters with significant first-order Sobol index values in all layers. The significance of MAXSMC in  
576 deeper layers is also evident in Fig 12, which shows the number of HRUs where a specific soil parameter is the  
577 most sensitive across three seasons at every soil layer. Soil porosity (MAXSMC) plays a crucial role in  
578 determining the water-holding capacity of the soil, the movement of water within the soil and ultimately runoff  
579 and evaporation, thus exerting a dominant control over soil moisture. (Arsenault et al., 2018; Cuntz et al., 2016).  
580 For the same reason, the dominance of MAXSMC increases in the deeper layers, even in the dry months (October  
581 to May). Further, the difference in the Sobol index values of parameters is minimal in deeper layers. This could  
582 be a reason for the systematic influence (high bias of VHet simulations compared to VHom) on rootzone soil  
583 moisture (Fig.11).

584 WLTSMC is another parameter that has significance on soil moisture till layer 3. During monsoon and at the  
585 surface layer, WLTSMC has  $S_T = 0.8$  and is equally significant parameter as MAXSMC across the watershed.  
586 During January-May, interactions between the parameters are limited across the layers, with minimal interaction  
587 at the surface. In these months, WLTSMC has some significance till layer 3, with the first-order Sobol index value  
588 greater than 0.1. WLTSMC controls stomatal resistance and, subsequently, the water availability for transpiration  
589 (Arsenault et al., 2018). Consequently, WLTSMC becomes significant only during the monsoon and afterward,  
590 as in Fig.12 and Fig.13, when sufficient water is available for plants, or LAI is prominent. In deeper layers below  
591 60 cm from the surface, the importance of WLTSMC is reduced significantly because the model simulations are  
592 parameterized to have root depth NROOT up to the third layer. Beyond this, the transpiration process is not  
593 considered; hence, its dominance was reduced. This also emphasizes the importance of the parameter root depth  
594 and the necessity of introducing a dynamic root depth when the focus is on hyper-resolution soil moisture  
595 simulation, especially in regions of fragmented agricultural systems (Gayler et al., 2014; Liu et al., 2020; Niu et  
596 al., 2020).

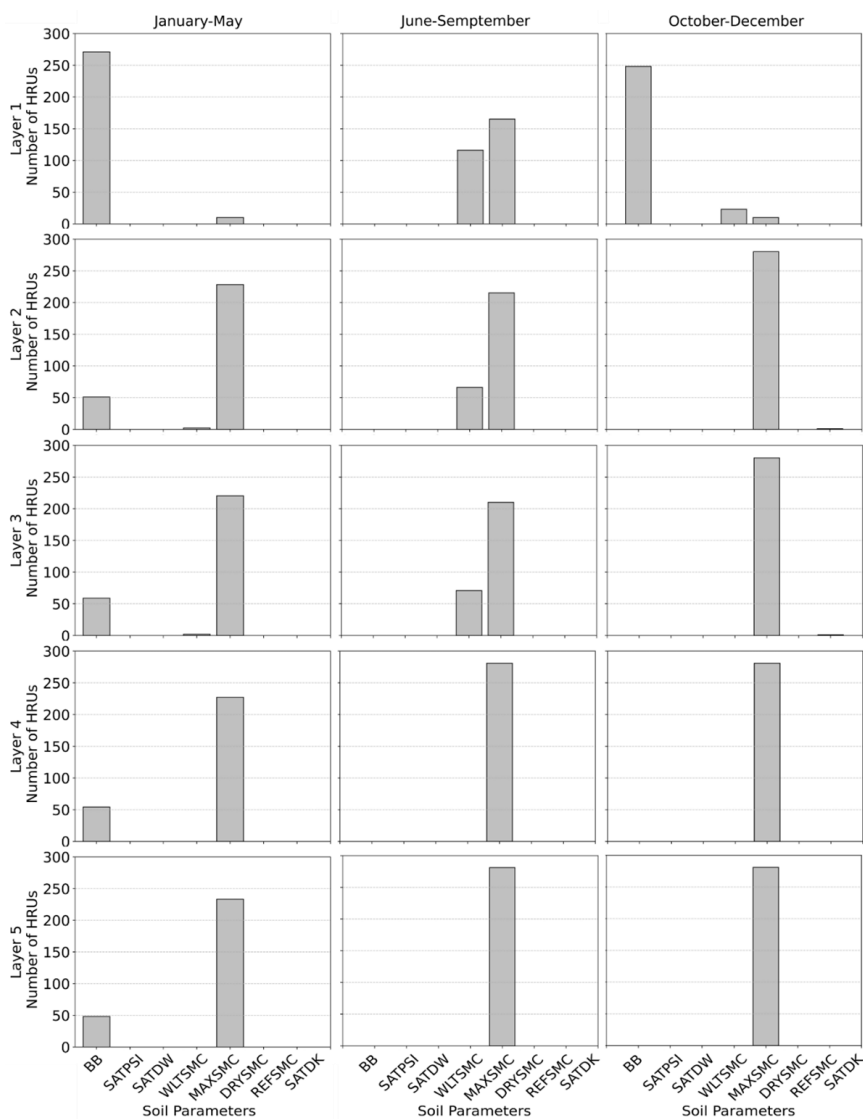


597 BB is another significant soil parameter for soil moisture simulation, particularly in the surface layer. During  
598 January -May, BB shows high sensitivity ( $S_T = 0.7$ ) at the surface with minimal interactions, as shown in Fig.13  
599 and Fig.13. During this season, transpiration loss in most months is zero as LAI used in the period accounts for  
600 zero, and runoff is minimal with limited precipitation events. Hence, any isolated precipitation events can induce  
601 evaporation, causing some variability in surface soil moisture, as shown in Fig.3. The parameter BB indicates the  
602 pore size distribution, which defines a relationship between soil moisture and matric potential, and in defining  
603 saturated hydraulic conductivity (SATDK), and diffusivity of soil water at saturation (SATDW). Hence, the  
604 parameter BB is also significant in deciding the loss of water from the surface layer, either percolating to the sub-  
605 surface layers and contributing to sub-surface runoff or evaporation (Cuntz et al., 2016) and is thus crucial in  
606 simulating surface layer soil moisture. During monsoon, with more precipitation events and vegetation, this  
607 exponential parameter (BB) interacts with other parameters, including MAXSMC, SATDK, and SATDK, causing  
608 it to be a sensitive soil parameter in terms of total-order Sobol index rather than first-order (Fig.12). Its influence  
609 on soil moisture dynamics is also evident during the post-monsoon season, October to December, where it  
610 interacts with other soil parameters, although less than that during monsoon.



611

612 **Figure 12:** Sensitivity of the Noah-MP soil parameters on an HRU within the SMAP pixel (green box in the  
 613 watershed map), used in the time series plots of watershed 20, to identify the influence of soil parameters across  
 614 different seasons at every layer. The first-order Sobol index,  $S_i$ , (light colour bar), indicates the parameter  
 615 contribution (no interaction with other parameters) to the total variance in soil moisture output. The total-order  
 616 Sobol index,  $S_T$  (darker colour bar), indicates the parameter contribution, including its interaction with other  
 617 parameters with respect to the total variance in soil moisture output.



618

619 **Figure 13:** Distribution of HRUs where a particular soil parameter exhibits the highest sensitivity (total-order  
 620 Sobol index) across three distinct seasons, as determined by sensitivity testing on watershed 20 at HRU scale  
 621 conducted at various soil layers with all the HRUs within the watershed.

622 **3.5 The added value of hyper-resolution modeling and vertical soil properties for small-sized farms**

623 HydroBlocks simulations have improved spatial heterogeneity of soil moisture at the surface ( $\sigma_0$ , of  $V_{Het} = 0.088$   
 624  $m^3m^{-3}$  and  $V_{Hom} = 0.084 m^3m^{-3}$ ) and rootzone ( $\sigma_0$ , of  $V_{Het} = 0.093 m^3m^{-3}$  and  $V_{Hom} = 0.09 m^3m^{-3}$ ) while  
 625 maintaining temporal consistency to macroscale products. As previously mentioned, the fragmented agricultural  
 626 system in India leads to significant diversity in agricultural practices. Consequently, there is substantial sub-grid  
 627 heterogeneity in irrigation requirements as well (Gumma et al., 2024). With improved subgrid heterogeneity of



628 soil moisture simulations (Fig. 5(b) and Fig.6(b)), HydroBlocks, as a hyper-resolution LSM, can cater to the  
629 demands of field-scale agricultural applications. The climatological conditions of the present study area,  
630 characterized by arid conditions and limited precipitation events, demand effective water management practices,  
631 which have global relevance. Hyper-resolution soil moisture with sub-grid heterogeneity can provide information  
632 regarding crop water deficiency, and with precision agriculture, water management practices can be improved  
633 (Peng et al., 2021).

634 HydroBlocks VHet simulations reveal that the deeper layer soil properties have a systematic influence (evident  
635 from high bias in Fig.10) at the rootzone and random influence at the surface layer (evident from high ubRMSD  
636 in Fig.11). At field scale soil properties are crucial in determining the spatial heterogeneity of soil moisture (Crow  
637 et al., 2012; Vergopolan et al., 2022). Incorporating vertical soil properties in the model better represents the  
638 ground reality, and the results reveal that VHet of soil can improve the rootzone soil moisture simulations.  
639 HydroBlocks VHet has higher spatial and subgrid variability than VHom at rootzone soil moisture (Fig.5(b) and  
640 Fig.6(b)). Developing a hyper-resolution LSM for farm scale soil moisture requires key improvement in several  
641 aspects including improved representation of surface and subsurface interactions (Wood et al., 2011). The  
642 HydroBlocks configurations used in the current study are limited by a lack of surface water routing, subsurface  
643 lateral connectivity during unsaturated conditions, dynamic representation of LAI and root depth, as well as  
644 improved topographical representation. Incorporating vertical soil properties in the model is one of the critical  
645 steps to achieve improved rootzone soil moisture simulations. Accurate estimates of rootzone soil moisture are  
646 critical for understanding and forecasting droughts (Ochsner et al., 2013). With their coarse resolution, traditional  
647 dynamic models have limited capability to capture field-scale variation in drought events (Abolafia-Rosenzweig  
648 et al., 2023). High-quality soil moisture data at the field scale can provide improved spatial heterogeneity,  
649 benefiting small-holding farmers (Peng et al., 2021; Vergopolan et al., 2021) through early warning of extreme  
650 events and thus reducing the crop loss risk.

#### 651 **4. Conclusions**

652 Recent studies proved the necessity of understanding horizontal and vertical soil heterogeneity in simulating  
653 hyper-resolution surface soil moisture (Vergopolan et al., 2022; Xu et al., 2023). Considering the importance of  
654 rootzone soil moisture in agriculture and India's fragmented agricultural system, this study implemented soil  
655 vertical heterogeneity in the hyper-resolution LSM to simulate surface and rootzone soil moisture in a  
656 predominantly cropland area in India for the first time. Since a field observation network for soil moisture in this  
657 study area was in progress, we assessed the performance of HydroBlocks against an available in situ station data,  
658 as well as SMAP L3 observations and SMAP L4 data for surface and rootzone soil moisture, respectively. The  
659 results from our study point out the following:

- 660 • At the field scale, HydroBlocks simulations with vertically homogeneous and vertically heterogeneous soil  
661 properties show improved spatial heterogeneity (for surface,  $\sigma_0$ , of VHet = 0.088  $\text{m}^3\text{m}^{-3}$  and VHom = 0.084  
662  $\text{m}^3\text{m}^{-3}$ ; for the rootzone,  $\sigma_0$ , of VHet = 0.093  $\text{m}^3\text{m}^{-3}$  and VHom = 0.09  $\text{m}^3\text{m}^{-3}$ ) compared to the macroscale  
663 products dataset. This is accomplished by considering various interactions between different physical  
664 controls, including topography, precipitation, land cover, and soil properties at the finer scale (Vergopolan  
665 et al., 2022)



- 666 • Evaluation against in situ data revealed that both VHet and VHom simulations performed similarly toward  
667 surface soil moisture simulation. However, VHet systematically improves soil moisture simulation than  
668 VHom by reducing the bias at all sub-surface layers. In the deeper layer (0-60 cm), VHet simulations show  
669 low bias ( $0.059 \text{ m}^3\text{m}^{-3}$ ) similar ubRMSE ( $0.066 \text{ m}^3\text{m}^{-3}$ ) and higher Pearson's correlation (0.60) than VHom  
670 with performance metrics of  $0.067 \text{ m}^3\text{m}^{-3}$ ,  $0.066 \text{ m}^3\text{m}^{-3}$  and 0.59 respectively.
- 671 • The 30m resolution HydroBlocks (VHet and VHom) simulations upscaled to ~10 km resolution showed a  
672 temporal pattern consistent with SMAP data. When evaluated against SMAP L3 observations and SMAP L4  
673 data, both model configurations performed well in terms of bias ( $0.02 \text{ m}^3\text{m}^{-3}$ ,  $0.021 \text{ m}^3\text{m}^{-3}$ ), ubRMSE ( $0.053$   
674  $\text{m}^3\text{m}^{-3}$ ,  $0.052 \text{ m}^3\text{m}^{-3}$ ), and Pearson's correlation (0.85, 0.85) for surface soil moisture and bias ( $0.056 \text{ m}^3\text{m}^{-3}$   
675  $^3$ ,  $0.049 \text{ m}^3\text{m}^{-3}$ ), ubRMSE ( $0.046 \text{ m}^3\text{m}^{-3}$ ,  $0.045 \text{ m}^3\text{m}^{-3}$ ), and Pearson's correlation (0.83, 0.85) for rootzone  
676 soil moisture.
- 677 • Comparison between HydroBlocks vertically homogeneous and vertically heterogeneous simulations reveal  
678 that deeper layer soil properties have a random influence on surface soil moisture and have a systematic  
679 influence on deeper layer soil moisture. Results also indicated that the influence of soil properties on  
680 rootzone soil moisture follows a topographical variation.
- 681 • Soil porosity (MAXSMC), the wilting point (WLTSMC), and Brooks-Corey parameter (BB) are crucial  
682 parameters influencing soil moisture at every layer and season. However, there is a season-wise variation in  
683 the interaction between soil parameters, which is more significant during monsoon than in other seasons.
- 684 • Sensitivity analysis across soil layers indicates a transition in the significance of soil parameters between the  
685 surface and deeper layers, with the order of significance remaining consistent between the deeper layers  
686 (below 30 cm from the surface). However, the exactness of such an influence requires an in-depth analysis  
687 in the future. Hence, incorporating soil vertical heterogeneity in LSMs is critical to the reliability of rootzone  
688 soil moisture simulations at a farm scale.

689 Although this study is limited by the lack of network of in situ observations to validate the simulations, comparison  
690 with the only in-situ observation available yielded promising results on the quality of simulations. Acknowledging  
691 this limitation, pertaining to in situ validation, we assessed the importance of hyper-resolution LSM in soil  
692 moisture simulation for farm-scale studies by comparing the simulations with available satellite-based soil  
693 moisture products, and analyzed the sensitivity of different model configurations and the importance of soil  
694 properties in simulating multi-layer soil moisture at farm scales. The current study uses lookup table of LAI values,  
695 which depicts variability during and post monsoon seasons. Incorporating dynamic LAI and dynamic root depth  
696 can improve soil moisture simulations (Liu et al., 2020; Niu et al., 2020). Future studies will focus on bringing  
697 LAI at the HRU scale and adopting a dynamic LAI scheme in the model. Further understanding the influence of  
698 topography and improving its parametrization to suit hyper-resolution is also necessary for improving soil  
699 moisture simulations.

#### 700 **Acknowledgments**

701 We acknowledge funding support from the project under the Ministry of Earth Sciences (MoES) Project ID:  
702 MoES/PAMC/H&C/148/2021/PC-II. India Meteorological Department is acknowledged for providing in situ soil  
703 moisture data for this study. We also acknowledge the efforts of Dr.Mangesh and Dr. Madhusudhan from the  
704 Indian Institute of Tropical Meteorology, Ministry of Earth Sciences, Government of India, for handling and  
705 processing in situ soil moisture data.



706 **Code and Data availability**

707 IMD in situ observations are available on request from <https://dsp.imdpune.gov.in/>, ERA5-Land soil moisture:  
708 <https://cds.climate.copernicus.eu/datasets/reanalysis-era5-land/> (Muñoz-Sabater et al., 2021), SMAP L3  
709 enhanced surface soil moisture: <https://doi.org/10.5067/4DQ54OUIJ9DL> (O'Neill et al., 2021), SMAP L4  
710 rootzone soil moisture: <https://doi.org/10.5067/60HB8VIP2T8W> (Reichle et al., 2014), GLEAM v3.6 surface and  
711 rootzone soil moisture: <https://www.gleam.eu/> (Martens et al., 2017), SoilGrids soil data: <https://soilgrids.org/>  
712 (Hengl et al., 2017), HydroBlocks source code: [https://github.com/chaneyn/HydroBlocks/tree/dev\\_noemi](https://github.com/chaneyn/HydroBlocks/tree/dev_noemi),  
713 (Chaney et al., 2016).

714

715 **Author contributions**

716 VK was responsible for the conceptualization, methodology, data processing and analysis, model development,  
717 prepared the manuscript-original draft including all figures, and led the writing of the paper with contributions  
718 from all the co-authors. KL, and JI were responsible for the conceptualization, supervision, and methodology of  
719 the study and writing -review and editing of the manuscript. NV was responsible for the supervision, software,  
720 writing -review, and editing of the manuscript. BBS provided in situ data for validation and writing -review and  
721 editing of the manuscript.

722 **Competing Interests**

723 None of the authors have competing interests.

724

725 **References**

- 726 Abolafia-Rosenzweig, R., He, C., Chen, F., Ikeda, K., Schneider, T., and Rasmussen, R.: High Resolution  
727 Forecasting of Summer Drought in the Western United States, *Water Resources Research*, 59,  
728 e2022WR033734, <https://doi.org/10.1029/2022WR033734>, 2023.
- 729 Arsenault, K. R., Nearing, G. S., Wang, S., Yatheendradas, S., and Peters-Lidard, C. D.: Parameter Sensitivity of  
730 the Noah-MP Land Surface Model with Dynamic Vegetation, *Journal of Hydrometeorology*, 19, 815–  
731 830, <https://doi.org/10.1175/jhm-d-17-0205.1>, 2018.
- 732 Baker, J. C. A., Garcia-Carreras, L., Gloor, M., Marsham, J. H., Buermann, W., da Rocha, H. R., Nobre, A. D.,  
733 de Araujo, A. C., and Spracklen, D. V.: Evapotranspiration in the Amazon: spatial patterns, seasonality,  
734 and recent trends in observations, reanalysis, and climate models, *Hydrology and Earth System Sciences*,  
735 25, 2279–2300, <https://doi.org/10.5194/hess-25-2279-2021>, 2021.
- 736 Benson, D. O. and Dirmeyer, P. A.: Characterizing the Relationship between Temperature and Soil Moisture  
737 Extremes and Their Role in the Exacerbation of Heat Waves over the Contiguous United States,  
738 <https://doi.org/10.1175/JCLI-D-20-0440.1>, 2021.
- 739 Cai, X., Yang, Z.-L., Xia, Y., Huang, M., Wei, H., Leung, L. R., and Ek, M. B.: Assessment of simulated water  
740 balance from Noah, Noah-MP, CLM, and VIC over CONUS using the NLDAS test bed, *Journal of*  
741 *Geophysical Research: Atmospheres*, 119, 13,751–13,770, <https://doi.org/10.1002/2014JD022113>, 2014.
- 742 Chaney, N. W., Metcalfe, P., and Wood, E. F.: HydroBlocks: a field-scale resolving land surface model for  
743 application over continental extents, *Hydrol. Process.*, 30, 3543–3559,  
744 <https://doi.org/10.1002/hyp.10891>, 2016.
- 745 Chaney, N. W., Torres-Rojas, L., Vergopolan, N., and Fisher, C. K.: HydroBlocks v0.2: enabling a field-scale  
746 two-way coupling between the land surface and river networks in Earth system models, *Geosci. Model*  
747 *Dev.*, 14, 6813–6832, <https://doi.org/10.5194/gmd-14-6813-2021>, 2021.
- 748 Chaubell, J., Yueh, S., Entekhabi, D., and Peng, J.: Resolution enhancement of SMAP radiometer data using the  
749 Backus Gilbert optimum interpolation technique, in: 2016 IEEE International Geoscience and Remote  
750 Sensing Symposium (IGARSS), 2016 IEEE International Geoscience and Remote Sensing Symposium  
751 (IGARSS), 284–287, <https://doi.org/10.1109/IGARSS.2016.7729065>, 2016.





- 752 Crow, W. T., Berg, A. A., Cosh, M. H., Loew, A., Mohanty, B. P., Panciera, R., de Rosnay, P., Ryu, D., and  
753 Walker, J. P.: Upscaling sparse ground-based soil moisture observations for the validation of coarse-  
754 resolution satellite soil moisture products, *Reviews of Geophysics*, 50,  
755 <https://doi.org/10.1029/2011RG000372>, 2012.
- 756 Cuntz, M., Mai, J., Samaniego, L., Clark, M., Wulfmeyer, V., Branch, O., Attinger, S., and Thober, S.: The impact  
757 of standard and hard-coded parameters on the hydrologic fluxes in the Noah-MP land surface model:  
758 HARD-CODED PARAMETERS IN NOAH-MP, *J. Geophys. Res. Atmos.*, 121, 10,676–10,700,  
759 <https://doi.org/10.1002/2016JD025097>, 2016.
- 760 Dai, Y., Shangguan, W., Wei, N., Xin, Q., Yuan, H., Zhang, S., Liu, S., Lu, X., Wang, D., and Yan, F.: A review  
761 of the global soil property maps for Earth system models, *SOIL*, 5, 137–158, [https://doi.org/10.5194/soil-](https://doi.org/10.5194/soil-5-137-2019)  
762 [5-137-2019](https://doi.org/10.5194/soil-5-137-2019), 2019.
- 763 Ding, J. and Zhu, Q.: The accuracy of multisource evapotranspiration products and their applicability in  
764 streamflow simulation over a large catchment of Southern China, *Journal of Hydrology: Regional  
765 Studies*, 41, 101092, <https://doi.org/10.1016/j.ejrh.2022.101092>, 2022.
- 766 Ek, M. B., Mitchell, K. E., Lin, Y., Rogers, E., Grunmann, P., Koren, V., Gayno, G., and Tarpley, J. D.:  
767 Implementation of Noah land surface model advances in the National Centers for Environmental  
768 Prediction operational mesoscale Eta model, *Journal of Geophysical Research: Atmospheres*, 108,  
769 <https://doi.org/10.1029/2002JD003296>, 2003.
- 770 Famiglietti, J. S., Ryu, D., Berg, A. A., Rodell, M., and Jackson, T. J.: Field observations of soil moisture  
771 variability across scales, *Water Resources Research*, 44, <https://doi.org/10.1029/2006WR005804>, 2008.
- 772 Garg, K. K., Bharati, L., Gaur, A., George, B., Acharya, S., Jella, K., and Narasimhan, B.: Spatial Mapping of  
773 Agricultural Water Productivity Using the Swat Model in Upper Bhima Catchment, India, *Irrigation and  
774 Drainage*, 61, 60–79, <https://doi.org/10.1002/ird.618>, 2012.
- 775 Gaur, N. and Mohanty, B. P.: Evolution of physical controls for soil moisture in humid and subhumid watersheds,  
776 *Water Resources Research*, 49, 1244–1258, <https://doi.org/10.1002/wrcr.20069>, 2013.
- 777 Gaur, N. and Mohanty, B. P.: Land-surface controls on near-surface soil moisture dynamics: Traversing remote  
778 sensing footprints, *Water Resources Research*, 52, 6365–6385, <https://doi.org/10.1002/2015WR018095>,  
779 2016.
- 780 Gayler, S., Wöhling, T., Grzeschik, M., Ingwersen, J., Wizemann, H.-D., Warrach-Sagi, K., Högy, P., Attinger,  
781 S., Streck, T., and Wulfmeyer, V.: Incorporating dynamic root growth enhances the performance of  
782 Noah-MP at two contrasting winter wheat field sites, *Water Resources Research*, 50, 1337–1356,  
783 <https://doi.org/10.1002/2013WR014634>, 2014.
- 784 Goswami, M.M., Mujumdar, M., Singh, B.B., Ingale, M., Ganeshi, N., Ranalkar, M., Franz, T.E., Srivastav, P.,  
785 Niyogi, D., Krishnan, R. and Patil, S.N.: Understanding the soil water dynamics during excess and deficit  
786 rainfall conditions over the core monsoon zone of India. *Environmental Research Letters*, 18(11),  
787 p.114011, 2023.
- 788 Government of India. Agriculture Census 2015-16: All India Report on Number and Area of Operational  
789 Holdings. Ministry of Agriculture & Farmers Welfare, Department of Agriculture, Cooperation &  
790 Farmers Welfare, New Delhi, 2019.
- 791 Gumma, M. K., Panjala, P., Dubey, S. K., Ray, D. K., Murthy, C. S., Kadiyala, D. M., Mohammed, I., and Takashi,  
792 Y.: Spatial Distribution of Cropping Systems in South Asia Using Time-Series Satellite Data Enriched  
793 with Ground Data, *Remote Sensing*, 16, 2733, <https://doi.org/10.3390/rs16152733>, 2024.
- 794 Gunnell, Y.: Relief and climate in South Asia: the influence of the western ghats on the current climate pattern of  
795 peninsular India, *International Journal of Climatology*, 17, 1169–1182,  
796 [https://doi.org/10.1002/\(SICI\)1097-0088\(199709\)17:11<1169::AID-JOC189>3.0.CO;2-W](https://doi.org/10.1002/(SICI)1097-0088(199709)17:11<1169::AID-JOC189>3.0.CO;2-W), 1997.
- 797 Hengl, T., Jesus, J. M. de, Heuvelink, G. B. M., Gonzalez, M. R., Kilibarda, M., Blagotić, A., Shangguan, W.,  
798 Wright, M. N., Geng, X., Bauer-Marschallinger, B., Guevara, M. A., Vargas, R., MacMillan, R. A.,  
799 Batjes, N. H., Leenaars, J. G. B., Ribeiro, E., Wheeler, I., Mantel, S., and Kempen, B.: SoilGrids250m:  
800 Global gridded soil information based on machine learning, *PLOS ONE*, 12, e0169748,  
801 <https://doi.org/10.1371/journal.pone.0169748>, 2017.
- 802 Herman, J. and Usher, W.: SALib: An open-source Python library for Sensitivity Analysis, *Journal of Open  
803 Source Software*, 2, 97, <https://doi.org/10.21105/joss.00097>, 2017.



- 804 Holzman, M. E., Rivas, R., and Piccolo, M. C.: Estimating soil moisture and the relationship with crop yield using  
805 surface temperature and vegetation index, *International Journal of Applied Earth Observation and*  
806 *Geoinformation*, 28, 181–192, <https://doi.org/10.1016/j.jag.2013.12.006>, 2014.
- 807 Jalilvand, E., Abolafia-Rosenzweig, R., Tajrishy, M., and Das, N. N.: Evaluation of SMAP/Sentinel 1 High-  
808 Resolution Soil Moisture Data to Detect Irrigation Over Agricultural Domain, *IEEE Journal of Selected*  
809 *Topics in Applied Earth Observations and Remote Sensing*, 14, 10733–10747,  
810 <https://doi.org/10.1109/JSTARS.2021.3119228>, 2021.
- 811 Jalilvand, E., Abolafia-Rosenzweig, R., Tajrishy, M., Kumar, S. V., Mohammadi, M. R., and Das, N. N.: Is It  
812 Possible to Quantify Irrigation Water-Use by Assimilating a High-Resolution Satellite Soil Moisture  
813 Product?, *Water Resources Research*, 59, e2022WR033342, <https://doi.org/10.1029/2022WR033342>,  
814 2023.
- 815 Ji, P., Yuan, X., and Liang, X.-Z.: Do Lateral Flows Matter for the Hyperresolution Land Surface Modeling?,  
816 *Journal of Geophysical Research: Atmospheres*, 122, 12,077–12,092,  
817 <https://doi.org/10.1002/2017JD027366>, 2017.
- 818 Joshi, C. and Mohanty, B. P.: Physical controls of near-surface soil moisture across varying spatial scales in an  
819 agricultural landscape during SMEX02, *Water Resources Research*, 46,  
820 <https://doi.org/10.1029/2010WR009152>, 2010.
- 821 Karra, K., Kontgis, C., Statman-Weil, Z., Mazzariello, J. C., Mathis, M., and Brumby, S. P.: Global land use /  
822 land cover with Sentinel 2 and deep learning, in: 2021 IEEE International Geoscience and Remote  
823 Sensing Symposium IGARSS, 2021 IEEE International Geoscience and Remote Sensing Symposium  
824 IGARSS, 4704–4707, <https://doi.org/10.1109/IGARSS47720.2021.9553499>, 2021.
- 825 Karthikeyan, L. and Kumar, D. N.: A novel approach to validate satellite soil moisture retrievals using  
826 precipitation data, *Journal of Geophysical Research: Atmospheres*, 121, 11,516–11,535,  
827 <https://doi.org/10.1002/2016JD024829>, 2016.
- 828 Kim, J. and Mohanty, B. P.: Influence of lateral subsurface flow and connectivity on soil water storage in land  
829 surface modeling, *Journal of Geophysical Research: Atmospheres*, 121, 704–721,  
830 <https://doi.org/10.1002/2015JD024067>, 2016.
- 831 Kishné, A. Sz., Yimam, Y. T., Morgan, C. L. S., and Dornblaser, B. C.: Evaluation and improvement of the default  
832 soil hydraulic parameters for the Noah Land Surface Model, *Geoderma*, 285, 247–259,  
833 <https://doi.org/10.1016/j.geoderma.2016.09.022>, 2017.
- 834 Krakauer, N. Y., Li, H., and Fan, Y.: Groundwater flow across spatial scales: importance for climate modeling,  
835 *Environ. Res. Lett.*, 9, 034003, <https://doi.org/10.1088/1748-9326/9/3/034003>, 2014.
- 836 Lawrence, D. M., Oleson, K. W., Flanner, M. G., Thornton, P. E., Swenson, S. C., Lawrence, P. J., Zeng, X.,  
837 Yang, Z.-L., Levis, S., Sakaguchi, K., Bonan, G. B., and Slater, A. G.: Parameterization improvements  
838 and functional and structural advances in Version 4 of the Community Land Model, *Journal of Advances*  
839 *in Modeling Earth Systems*, 3, <https://doi.org/10.1029/2011MS00045>, 2011.
- 840 Lehner, B. and Grill, G.: Global river hydrography and network routing: baseline data and new approaches to  
841 study the world's large river systems, *Hydrological Processes*, 27, 2171–2186,  
842 <https://doi.org/10.1002/hyp.9740>, 2013.
- 843 Liu, X., Chen, F., Barlage, M., and Niyogi, D.: Implementing Dynamic Rooting Depth for Improved Simulation  
844 of Soil Moisture and Land Surface Feedbacks in Noah-MP-Crop, *Journal of Advances in Modeling Earth*  
845 *Systems*, 12, e2019MS001786, <https://doi.org/10.1029/2019MS001786>, 2020.
- 846 Martens, B., Miralles, D. G., Lievens, H., Van Der Schalie, R., De Jeu, R. A. M., Fernández-Prieto, D., Beck, H.  
847 E., Dorigo, W. A., and Verhoest, N. E. C.: GLEAM v3: satellite-based land evaporation and root-zone  
848 soil moisture, *Geosci. Model Dev.*, 10, 1903–1925, <https://doi.org/10.5194/gmd-10-1903-2017>, 2017.
- 849 Muñoz-Sabater, J., Dutra, E., Agustí-Panareda, A., Albergel, C., Arduini, G., Balsamo, G., Boussetta, S., Choulga,  
850 M., Harrigan, S., Hersbach, H., Martens, B., Miralles, D. G., Piles, M., Rodríguez-Fernández, N. J.,  
851 Zsoter, E., Buontempo, C., and Thépaut, J.-N.: ERA5-Land: a state-of-the-art global reanalysis dataset  
852 for land applications, *Earth System Science Data*, 13, 4349–4383, [https://doi.org/10.5194/essd-13-4349-](https://doi.org/10.5194/essd-13-4349-2021)  
853 2021, 2021.



- 854 Niu, G., Fang, Y., Chang, L., Jin, J., Yuan, H., and Zeng, X.: Enhancing the Noah-MP Ecosystem Response to  
855 Droughts With an Explicit Representation of Plant Water Storage Supplied by Dynamic Root Water  
856 Uptake, *J Adv Model Earth Syst*, 12, <https://doi.org/10.1029/2020MS002062>, 2020.
- 857 Niu, G.-Y., Yang, Z.-L., Dickinson, R. E., and Gulden, L. E.: A simple TOPMODEL-based runoff  
858 parameterization (SIMTOP) for use in global climate models, *Journal of Geophysical Research:*  
859 *Atmospheres*, 110, <https://doi.org/10.1029/2005JD006111>, 2005.
- 860 Niu, G.-Y., Yang, Z.-L., Mitchell, K. E., Chen, F., Ek, M. B., Barlage, M., Kumar, A., Manning, K., Niyogi, D.,  
861 Rosero, E., Tewari, M., and Xia, Y.: The community Noah land surface model with  
862 multiparameterization options (Noah-MP): 1. Model description and evaluation with local-scale  
863 measurements, *Journal of Geophysical Research: Atmospheres*, 116,  
864 <https://doi.org/10.1029/2010JD015139>, 2011.
- 865 Ochsner, T. E., Cosh, M. H., Cuenca, R. H., Dorigo, W. A., Draper, C. S., Hagimoto, Y., Kerr, Y. H., Larson, K.  
866 M., Njoku, E. G., Small, E. E., and Zreda, M.: State of the Art in Large-Scale Soil Moisture Monitoring,  
867 *Soil Science Society of America Journal*, 77, 1888–1919, <https://doi.org/10.2136/sssaj2013.03.0093>,  
868 2013.
- 869 O’Neill, P., Bindlish, R., Chan, S., Chaubell, J., Colliander, A., Njoku, E., and Jackson, T.: Algorithm Theoretical  
870 Basis Document Level 2 & 3 Soil Moisture (Passive) Data Products, 2021.
- 871 Park, S., Im, J., Park, S., and Rhee, J.: Drought monitoring using high resolution soil moisture through multi-  
872 sensor satellite data fusion over the Korean peninsula, *Agricultural and Forest Meteorology*, 237–238,  
873 257–269, <https://doi.org/10.1016/j.agrformet.2017.02.022>, 2017.
- 874 Pavelic, P., Patankar, U., Acharya, S., Jella, K., and Gumma, M. K.: Role of groundwater in buffering irrigation  
875 production against climate variability at the basin scale in South-West India, *Agricultural Water*  
876 *Management*, 103, 78–87, <https://doi.org/10.1016/j.agwat.2011.10.019>, 2012.
- 877 Peng, J., Albergel, C., Balenzano, A., Brocca, L., Cartus, O., Cosh, M. H., Crow, W. T., Dabrowska-Zielinska,  
878 K., Dadson, S., Davidson, M. W. J., de Rosnay, P., Dorigo, W., Gruber, A., Hagemann, S., Hirschi, M.,  
879 Kerr, Y. H., Lovergine, F., Mahecha, M. D., Marzahn, P., Mattia, F., Musial, J. P., Preuschmann, S.,  
880 Reichle, R. H., Satalino, G., Silgram, M., van Bodegom, P. M., Verhoest, N. E. C., Wagner, W., Walker,  
881 J. P., Wegmüller, U., and Loew, A.: A roadmap for high-resolution satellite soil moisture applications –  
882 confronting product characteristics with user requirements, *Remote Sensing of Environment*, 252,  
883 112162, <https://doi.org/10.1016/j.rse.2020.112162>, 2021.
- 884 Poggio, L., de Sousa, L. M., Batjes, N. H., Heuvelink, G. B. M., Kempen, B., Ribeiro, E., and Rossiter, D.:  
885 SoilGrids 2.0: producing soil information for the globe with quantified spatial uncertainty, *SOIL*, 7, 217–  
886 240, <https://doi.org/10.5194/soil-7-217-2021>, 2021.
- 887 Ray, S. S., Dadhwal, V. K., and Navalgund, R. R.: Progress and Challenges in Earth Observation Data  
888 Applications for Agriculture at Field Scale in India and Small Farm Holdings Regions, *J Indian Soc*  
889 *Remote Sens*, 50, 189–196, <https://doi.org/10.1007/s12524-022-01523-w>, 2022.
- 890 Reichle, R., Koster, R., Lannoy, G. D., Crow, W., and Kimball, J.: SMAP Algorithm Theoretical Basis Document:  
891 Level 4 Surface and Root Zone Soil Moisture (L4\_SM), JPL D-66483, 2014.
- 892 Rigden, A. J., Mueller, N. D., Holbrook, N. M., Pillai, N., and Huybers, P.: Combined influence of soil moisture  
893 and atmospheric evaporative demand is important for accurately predicting US maize yields, *Nat Food*,  
894 1, 127–133, <https://doi.org/10.1038/s43016-020-0028-7>, 2020.
- 895 Rosenbaum, U., Bogena, H. R., Herbst, M., Huisman, J. A., Peterson, T. J., Weuthen, A., Western, A. W., and  
896 Vereecken, H.: Seasonal and event dynamics of spatial soil moisture patterns at the small catchment  
897 scale, *Water Resources Research*, 48, <https://doi.org/10.1029/2011WR011518>, 2012.
- 898 Saxton, K. E. and Rawls, W. J.: Soil Water Characteristic Estimates by Texture and Organic Matter for Hydrologic  
899 Solutions, *Soil Science Society of America Journal*, 70, 1569–1578,  
900 <https://doi.org/10.2136/sssaj2005.0117>, 2006.
- 901 Schwingshackl, C., Hirschi, M., and Seneviratne, S. I.: A theoretical approach to assess soil moisture–climate  
902 coupling across CMIP5 and GLACE-CMIP5 experiments, *Earth System Dynamics*, 9, 1217–1234,  
903 <https://doi.org/10.5194/esd-9-1217-2018>, 2018.
- 904 Sehgal, V., Gaur, N., and Mohanty, B. P.: Global Surface Soil Moisture Drydown Patterns, *Water Resources*  
905 *Research*, 57, e2020WR027588, <https://doi.org/10.1029/2020WR027588>, 2021.



- 906 Singh, R. S., Reager, J. T., Miller, N. L., and Famiglietti, J. S.: Toward hyper-resolution land-surface modeling:  
907 The effects of fine-scale topography and soil texture on CLM4.0 simulations over the Southwestern U.S.,  
908 *Water Resources Research*, 51, 2648–2667, <https://doi.org/10.1002/2014WR015686>, 2015.
- 909 Tjrdeman, E. and Menzel, L.: The development and persistence of soil moisture stress during drought across  
910 southwestern Germany, *Hydrology and Earth System Sciences*, 25, 2009–2025,  
911 <https://doi.org/10.5194/hess-25-2009-2021>, 2021.
- 912 Torres-Rojas, L., Vergopolan, N., Herman, J. D., and Chaney, N. W.: Towards an Optimal Representation of Sub-  
913 Grid Heterogeneity in Land Surface Models, *Water Resources Research*, 58, e2022WR032233,  
914 <https://doi.org/10.1029/2022WR032233>, 2022.
- 915 Vergopolan, N., Chaney, N. W., Beck, H. E., Pan, M., Sheffield, J., Chan, S., and Wood, E. F.: Combining hyper-  
916 resolution land surface modeling with SMAP brightness temperatures to obtain 30-m soil moisture  
917 estimates, *Remote Sensing of Environment*, 242, 111740, <https://doi.org/10.1016/j.rse.2020.111740>,  
918 2020.
- 919 Vergopolan, N., Xiong, S., Estes, L., Wanders, N., Chaney, N. W., Wood, E. F., Konar, M., Caylor, K., Beck, H.  
920 E., Gatti, N., Evans, T., and Sheffield, J.: Field-scale soil moisture bridges the spatial-scale gap between  
921 drought monitoring and agricultural yields, *Hydrology and Earth System Sciences*, 25, 1827–1847,  
922 <https://doi.org/10.5194/hess-25-1827-2021>, 2021.
- 923 Vergopolan, N., Sheffield, J., Chaney, N. W., Pan, M., Beck, H. E., Ferguson, C. R., Torres-Rojas, L., Eigenbrod,  
924 F., Crow, W., and Wood, E. F.: High-Resolution Soil Moisture Data Reveal Complex Multi-Scale Spatial  
925 Variability Across the United States, *Geophysical Research Letters*, 49, e2022GL098586,  
926 <https://doi.org/10.1029/2022GL098586>, 2022.
- 927 Wood, E. F., Roundy, J. K., Troy, T. J., van Beek, L. P. H., Bierkens, M. F. P., Blyth, E., de Roo, A., Döll, P., Ek,  
928 M., Famiglietti, J., Gochis, D., van de Giesen, N., Houser, P., Jaffé, P. R., Kollet, S., Lehner, B.,  
929 Lettenmaier, D. P., Peters-Lidard, C., Sivapalan, M., Sheffield, J., Wade, A., and Whitehead, P.:  
930 Hyperresolution global land surface modeling: Meeting a grand challenge for monitoring Earth's  
931 terrestrial water, *Water Resources Research*, 47, <https://doi.org/10.1029/2010WR010090>, 2011.
- 932 Xu, C., Torres-Rojas, L., Vergopolan, N., and Chaney, N. W.: The Benefits of Using State-Of-The-Art Digital  
933 Soil Properties Maps to Improve the Modeling of Soil Moisture in Land Surface Models, *Water  
934 Resources Research*, 59, e2022WR032336, <https://doi.org/10.1029/2022WR032336>, 2023.
- 935 Yang, K., Koike, T., Ye, B., and Bastidas, L.: Inverse analysis of the role of soil vertical heterogeneity in  
936 controlling surface soil state and energy partition, *Journal of Geophysical Research: Atmospheres*, 110,  
937 <https://doi.org/10.1029/2004JD005500>, 2005.
- 938 Yang, Y., Peng, B., Guan, K., Pan, M., Franz, Trenton. E., Cosh, M. H., and Bernacchi, C. J.: Within-field soil  
939 moisture variability and time-invariant spatial structures of agricultural fields in the US Midwest, *Vadose  
940 Zone Journal*, 23, e20337, <https://doi.org/10.1002/vzj2.20337>, 2024.
- 941 Zhou, Y., Zaitchik, B. F., Kumar, S. V., Nie, W., Loomis, B. D., Richey McLarty, A. S., and Appana, R.: Satellite-  
942 informed simulation of irrigation in South Asia: Opportunities and uncertainties, *Journal of Hydrology*,  
943 641, 131758, <https://doi.org/10.1016/j.jhydrol.2024.131758>, 2024.
- 944 Zhu, J. and Mohanty, B. P.: Effective hydraulic parameters for steady state vertical flow in heterogeneous soils,  
945 *Water Resources Research*, 39, <https://doi.org/10.1029/2002WR001831>, 2003.
- 946 Zhu, W., Tian, S., Wei, J., Jia, S., and Song, Z.: Multi-scale evaluation of global evapotranspiration products  
947 derived from remote sensing images: Accuracy and uncertainty, *Journal of Hydrology*, 611, 127982,  
948 <https://doi.org/10.1016/j.jhydrol.2022.127982>, 2022.